Evaporation boundary conditions for the R13 equations of rarefied gas dynamics

Henning Struchtrup, Alexander Beckmann, Anirudh Singh Rana, and Aldo Frezzotti

Evaporation boundary conditions for the R13 equations of rarefied gas dynamics

Henning Struchtrup,[1,a)] Alexander Beckmann,[1] Anirudh Singh Rana,[2] and Aldo Frezzotti[3]

[1]*Department of Mechanical Engineering, University of Victoria, Victoria, British Columbia V8W 3P6, Canada*
[2]*Mathematics Institute, University of Warwick, Warwick, United Kingdom*
[3]*Dipartimento di Scienze and Tecnologie Aerospaziali, Politecnico di Milano, Milano, Italy*

The regularized 13 moment (R13) equations are a macroscopic model for the description of rarefied gas flows in the transition regime. The equations have been shown to give meaningful results for Knudsen numbers up to about 0.5. Here, their range of applicability is extended by deriving and testing boundary conditions for evaporating and condensing interfaces. The macroscopic interface conditions are derived from the microscopic interface conditions of kinetic theory. Tests include evaporation into a half-space and evaporation/condensation of a vapor between two liquid surfaces of different temperatures. Comparison indicates that overall the R13 equations agree better with microscopic solutions than classical hydrodynamics. © 2017 Author(s). All article content, except where otherwise noted, is licensed under a Creative Commons Attribution (CC BY) license (http://creativecommons.org/licenses/by/4.0/). [http://dx.doi.org/10.1063/1.4989570]

I. INTRODUCTION

The regularized 13 moment (R13) equations are a macroscopic model to describe rarefied gas flows for not too large Knudsen numbers in good approximation to the Boltzmann equation.[1–5] Gas rarefaction leads to the occurrence of phenomena such as velocity slip and temperature jump at boundaries, Knudsen layers in front of boundaries, transpiration flow, thermal stresses, or heat transfer without temperature gradients, all of which are reproduced by solutions of the R13 equations. Proper modeling of boundary conditions (BCs) is essential to obtain a meaningful description of rarefied flows, and below we develop and test conditions for liquid-vapor boundaries with condensation and evaporation. With this, the range of application of the R13 equations is extended in particular towards micro-devices with phase change; possible applications include, e.g., gas supply channels in micro-fuel cells.

Indeed, it is well known that rarefied gas flows cannot be accurately described by the Navier-Stokes-Fourier (NSF) equations of classical hydrodynamics.[3,6,7] While adding jump and slip boundary conditions to NSF introduces some of these effects into classical hydrodynamics, all bulk rarefaction effects remain elusive.[8] A fully accurate description of rarefied flow behavior requires solution of the Boltzmann equation, e.g., by the direct simulation Monte Carlo (DSMC) method[9] or by direct numerical simulation,[10] but typical computational times are often significantly above those for hydrodynamics, in particular, when the degree of rarefaction is mild. Macroscopic models for rarefied flows, such as the R13 equations, extend the equations of hydrodynamics by accounting for a small number of additional flow variables, yet describe bulk

rarefaction phenomena in good approximation, and thus offer an alternative tool for computation.[4,5]

The R13 equations are derived as approximations of the Boltzmann by means of the order of magnitude method,[11,12] which combines elements of the Chapman-Enskog[6] and Grad[13,14] methods. The resulting equations avoid the problems exhibited by the individual methods. Higher order Chapman-Enskog expansions yield the Burnett[15] and super-Burnett[16] equations, which are well known to be unstable in time dependent processes[17,18] and to give unphysical solutions in steady state.[19] Grad's 13 moment equations, or systems with more moments, are stable but exhibit unphysical sub-shocks for high speed flows.[20] Moreover, the Grad equations are not linked to the Knudsen number; hence, it is difficult to know *a priori* which set of moments should be considered for a given process. In contrast, the R13 equations are stable, have no sub-shocks, and are derived to be of third order in the Knudsen number (super-Burnett order).[12] The method can be extended to higher moment numbers.[21,22]

Details of the R13 equations depend on the molecular model, and in the following we consider only the well-established equations for Maxwell molecules.[12] Equations for hard sphere molecules,[23] polyatomic gases,[24] and gas mixtures[25] are discussed elsewhere in the literature.

Just as the transport equations are derived from the Boltzmann equation, the corresponding macroscopic boundary and interface conditions are derived from the microscopic boundary and interface conditions for the Boltzmann equation.[26] For this we use an extended Maxwell boundary model[27] with a condensation/evaporation coefficient (probability that a vapor particle condenses at impact on the liquid) and an accommodation coefficient (probability for diffuse vs. specular reflection for a non-condensing particle).[28] The derivation follows the same line as that of the wall boundary conditions for non-condensing interfaces. Naturally, for a vanishing

a)struchtr@uvic.ca. URL: http://www.engr.uvic.ca/~struchtr/

condensation coefficient, the boundary conditions for solid walls are recovered.

After deriving the full set of boundary conditions, as a first application, we solve two simple one-dimensional evaporation problems: a half-space problem for pressure driven evaporation[29,30] and condensation and evaporation of a vapor between two liquid surfaces at different interface temperatures.[31–35] For both cases, the R13 and NSF equations can be analytically solved, and their solutions are compared with DSMC simulations. The ability of the macroscopic models to model rarefied gas flows with evaporating or condensing interfaces is discussed.

While we discuss only one-dimensional problems as applications, the boundary conditions are developed for full three-dimensional geometry, and multi-dimensional problems will be considered in the future.

We note that in the present paper, we consider problems that focus on transport in the vapor, with given liquid data at the interface. The full simulation of problems involving liquid-vapor interface requires a matching model for the transport in the liquid, which for completeness is outlined in the Appendix A.

The remainder of the paper proceeds as follows: Sec. II will briefly review the R13 equations and their relation to kinetic theory, as well as to classical hydrodynamics. Based on this, the evaporation and condensation boundary conditions for the R13 equations will be derived in Sec. III from the corresponding boundary conditions for the Boltzmann equation. The relation of the extended R13 evaporation/condensation conditions to those for hydrodynamics, such as Hertz-Knudsen-Schrage, will be discussed as well. In Sec. IV, we solve simple one-dimensional evaporation problems—a half-space evaporation problem and heat and mass transfer between two liquid layers—with the R13 equations and compare results to kinetic theory simulations and results from classical hydrodynamics. The paper ends with our conclusions. Some preliminary results were published before;[36] the present contribution gives all required details for the derivation of the boundary conditions, corrects several errors, and expands on the results presented and discussed.

II. THE R13 EQUATIONS

A. Moments and moment equations

We briefly recall the origin of the R13 equations from kinetic theory of monatomic gases. The aim of kinetic theory is to find the velocity distribution function $f(x_i, t, c_i)$ which is defined such that $f(x_i, t, c_i)\,d\mathbf{c}d\mathbf{x}$ gives the number of particles in the phase space cell $d\mathbf{c}d\mathbf{x}$ at time t; x_i is the location in space and c_i is the microscopic velocity of a particle. In a microscopic approach, the distribution function is the solution of the Boltzmann equation,[6,7] while in a macroscopic approach, one derives transport equations as a set of suitable moments of the Boltzmann equation, where the resulting moment equations are closed by means of an ansatz for the distribution. This so-called moment method goes back to the work of Grad, and his 13 moment equations are the best known set of macroscopic equations.[13,14] The basic 13 variables are mass density ρ,

macroscopic velocity v_i, temperature T, anisotropic stress tensor σ_{ij} (with $\sigma_{ii} = 0$), and heat flux vector q_i, which are moments of the distribution function as

$$\rho = m \int f d\mathbf{c},$$
$$\rho v_i = m \int c_i f d\mathbf{c},$$
$$\rho u = \frac{3}{2}\rho\theta = \frac{m}{2}\int C^2 f d\mathbf{c}, \qquad (1)$$
$$\sigma_{ij} = m \int C_{\langle i}C_{j\rangle} f d\mathbf{c},$$
$$q_i = \frac{m}{2}\int C^2 C_i f d\mathbf{c}.$$

Here, $u = \frac{3}{2}RT = \frac{3}{2}\theta$ is the specific internal energy, $\theta = RT$ is temperature in specific energy units with the gas constant R, and $C_i = c_i - v_i$ is the peculiar velocity. Indices in angular brackets denote the symmetric and trace-free part of a tensor.[3]

The corresponding moment equations are the conservation laws for mass, momentum, and energy, which can be written as ($\frac{D}{Dt} = \frac{\partial}{\partial t} + v_k \frac{\partial}{\partial x_k}$ is the material time derivative)

$$\frac{D\rho}{Dt} + \rho\frac{\partial v_k}{\partial x_k} = 0,$$

$$\rho\frac{Dv_i}{Dt} + \rho\frac{\partial\theta}{\partial x_i} + \theta\frac{\partial\rho}{\partial x_i} + \frac{\partial\sigma_{ik}}{\partial x_k} = 0, \qquad (2)$$

$$\frac{3}{2}\rho\frac{D\theta}{Dt} + \rho\theta\frac{\partial v_k}{\partial x_k} + \frac{\partial q_k}{\partial x_k} + \sigma_{kl}\frac{\partial v_k}{\partial x_l} = 0,$$

and the balance equations for stress and heat flux

$$\frac{D\sigma_{ij}}{Dt} + \sigma_{ij}\frac{\partial v_k}{\partial x_k} + 2\sigma_{k\langle i}\frac{\partial v_{j\rangle}}{\partial x_k} + \frac{4}{5}\frac{\partial q_{\langle i}}{\partial x_{j\rangle}} + \frac{\partial m_{ijk}}{\partial x_k}$$
$$= -\rho\theta\left[\frac{\sigma_{ij}}{\mu} + 2\frac{\partial v_{\langle i}}{\partial x_{j\rangle}}\right], \qquad (3)$$

$$\frac{Dq_i}{Dt} + \frac{5}{2}\sigma_{ik}\frac{\partial\theta}{\partial x_k} - \sigma_{ik}\theta\frac{\partial\ln\rho}{\partial x_k} + \theta\frac{\partial\sigma_{ik}}{\partial x_k} + \frac{7}{5}q_i\frac{\partial v_k}{\partial x_k} + \frac{7}{5}q_k\frac{\partial v_i}{\partial x_k}$$
$$+ \frac{2}{5}q_k\frac{\partial v_k}{\partial x_i} + \frac{1}{2}\frac{\partial R_{ik}}{\partial x_k} + \frac{1}{6}\frac{\partial\Delta}{\partial x_i} + m_{ikl}\frac{\partial v_k}{\partial x_l} - \frac{\sigma_{ik}}{\rho}\frac{\partial\sigma_{kl}}{\partial x_l}$$
$$= -\frac{5}{2}\rho\theta\left[\frac{q_i}{\kappa} + \frac{\partial\theta}{\partial x_i}\right]. \qquad (4)$$

The collision terms of the above equations were determined for Maxwell molecules, μ is the shear viscosity and $\kappa = \frac{15}{4}\mu$ is the heat conductivity.[3]

For small Knudsen numbers, the Chapman-Enskog method[3,6] can be used to reduce the equations for stress and heat flux to the Navier-Stokes and Fourier laws,

$$\sigma_{ij} = -2\mu\frac{\partial v_{\langle i}}{\partial x_{j\rangle}}, \quad q_i = -\kappa\frac{\partial\theta}{\partial x_i}. \qquad (5)$$

B. Constitutive equations

In addition to the 13 variables introduced above, the 13 moment equations (2)–(4) contain the higher moments,

$$m_{ijk} = m \int C_{\langle i} C_j C_{k \rangle} f d\mathbf{c},$$

$$\Delta = m \int C^4 f d\mathbf{c} - 15\rho\theta^2, \qquad (6)$$

$$R_{ij} = m \int C^2 C_{\langle i} C_{j \rangle} f d\mathbf{c} - 7\theta\sigma_{ij}.$$

In order to close the system of moment equations, constitutive equations for these must be provided. The classical Grad closure[3,13] simply leads to

$$m_{ijk|G} = \Delta_{|G} = R_{ij|G} = 0. \qquad (7)$$

The regularized 13 moment equations arise from an alternative closure,[1] which accounts for parts of, but not the complete, transport equations for $\{m_{ijk}, \Delta, R_{ij}\}$. The equations are best derived by means of the order of magnitude method,[11,12] which mixes elements of the Grad and Chapman-Enskog methods to find the relevant terms of the infinite moment system that are required to have accuracy at a certain order in the Knudsen number, which is defined as $\mathrm{Kn} = \frac{\mu\sqrt{\theta}}{pL}$, where L is the relevant macroscopic length.[3] The regularized 13 moment equations arise as the appropriate set of equations at 3rd order in the Knudsen number (super-Burnett order) and consist of Eqs. (2)–(4) and the constitutive equations (pressure obeys the ideal gas law, $p = \rho\theta$),

$$\Delta = 5\frac{\sigma_{kl}\sigma_{kl}}{\rho} + \frac{56}{5}\frac{q_k q_k}{p} - 12\mu\theta\frac{\partial}{\partial x_k}\left(\frac{q_k}{p}\right),$$

$$R_{ij} = \frac{20}{7}\frac{\sigma_{k\langle i}\sigma_{j\rangle k}}{\rho} + \frac{64}{25}\frac{q_{\langle i}q_{j\rangle}}{p} - \frac{24}{5}\mu\theta\frac{\partial}{\partial x_{\langle i}}\left(\frac{q_{j\rangle}}{p}\right), \qquad (8)$$

$$m_{ijk} = \frac{4}{3}\frac{\sigma_{\langle ij}q_{k\rangle}}{p} - 2\mu\theta\frac{\partial}{\partial x_{\langle i}}\left(\frac{\sigma_{jk\rangle}}{p}\right).$$

Some comments regarding the closure are in order: First, the closure depends on the molecular model employed in the Boltzmann equation and is performed easiest for Maxwell molecules, which results in the coefficients as given above. For other molecular models, the transport equations, and the coefficients in the closure, change. This was discussed in Ref. 23, where the linear transport equations for hard sphere molecules were derived. Non-linear second order (i.e., Burnett order) equations for hard sphere molecules were derived before;[3,11] these could be combined with the linear regularization at third order to give a non-linear system of equations for non-Maxwellian molecules; this will be discussed elsewhere.

Second, the order of magnitude method allows for some ambiguity of the equations, since it aims only for the proper terms at a given Knudsen order. Since the R13 equations are of third order in Kn, one can modify them in a way that the third order contributions remain unchanged, while higher order contributions change. Over the years, this ambiguity has led to several versions of the R13 equations presented in the literature. The first derivation[1] of the R13 equations relied on the artificial assumption that higher moments would change on a faster time scale and a Chapman-Enskog expansion for the fast scale; the resulting equations include some terms that contribute at the fourth order in Kn, which, one can argue, should not be present in a third order theory. The re-derivation by

means of the order of magnitude method removed these fourth order terms.[12] Even then, the number of boundary conditions required for the solution of the equations differed between the linear and the non-linear equations.[26] For the closure presented (8), the equations were modified such that linear and non-linear equations require the same number of boundary conditions,[37] and this is the preferred version of the R13 equations for slow flows. For non-linear processes such as shock waves, various versions show marked differences in the results.[38]

Since the full Boltzmann collision term is difficult to handle, many authors base numerical simulation of rarefied gas flows on the Bhatnagar–Gross–Krook (BGK) model,[39] which approximates the Boltzmann collision term with a rate ansatz. Qualitatively, the BGK model gives an accurate description of rarefied gas flows, but due to its simplicity, it does not lead to quantitative agreement; most prominently, it gives a wrong value for the Prandtl number.[3,7] In order to be able to compare our description of evaporation/condensation processes in rarefied flows with BGK solutions, we occasionally consider the R13 equations for the BGK model, where the heat conductivity is $\kappa_{\mathrm{BGK}} = \frac{5}{2}\mu$, and the closure relations are similar to the above but have different coefficients in almost all terms,[12]

$$\Delta^{\mathrm{BGK}} = 4\frac{\sigma_{kl}\sigma_{kl}}{\rho} + \frac{56}{5}\frac{q_k q_k}{p} - 8\mu\theta\frac{\partial}{\partial x_k}\left(\frac{q_k}{p}\right),$$

$$R_{ij}^{\mathrm{BGK}} = 4\frac{\sigma_{k\langle i}\sigma_{j\rangle k}}{\rho} + \frac{56}{5}\frac{q_{\langle i}q_{j\rangle}}{p} - \frac{28}{5}\mu\theta\frac{\partial}{\partial x_{\langle i}}\left(\frac{q_{j\rangle}}{p}\right), \qquad (9)$$

$$m_{ijk}^{\mathrm{BGK}} = \frac{12}{5}\frac{\sigma_{\langle ij}q_{k\rangle}}{p} - 3\mu\theta\frac{\partial}{\partial x_{\langle i}}\left(\frac{\sigma_{jk\rangle}}{p}\right).$$

C. Distribution function in the bulk

At a physical boundary, such as a wall or a phase boundary, the distribution function of incoming particles changes due to reflection, condensation, and evaporation.[26,28] To derive boundary conditions for moments from the boundary conditions for the phase density, a detailed expression for the distribution function in terms of the moments is required. For this we use the same distribution that is used for the closure of the moment system, namely, the Grad distribution for the 26 moments (1, 6). The Grad-26 moment distribution is the local equilibrium distribution f_M times a suitable polynomial,[3]

$$f_{|G26} = f_M\left(1 + \frac{\Delta}{8p\theta}\left(1 - \frac{2}{3}\frac{C^2}{\theta} + \frac{1}{15}\frac{C^4}{\theta^2}\right)\right.$$

$$+ \frac{2}{5}\frac{q_k}{p\theta}C_k\left(\frac{C^2}{2\theta} - \frac{5}{2}\right) + \frac{\sigma_{ij}}{2p\theta}C_{\langle i}C_{j\rangle}$$

$$\left. - \frac{R_{ij}}{4p\theta^2}C_{\langle i}C_{j\rangle}\left(1 - \frac{1}{7}\frac{C^2}{\theta}\right) + \frac{m_{ijk}}{6\rho\theta^3}C_{\langle i}C_jC_{k\rangle}\right), \qquad (10)$$

where the equilibrium function is the local Maxwellian

$$f_M(p, \theta, C) = \frac{p}{m\theta}\frac{1}{(2\pi\theta)^{3/2}}\exp\left(-\frac{C^2}{2\theta}\right). \qquad (11)$$

Insertion of this distribution into the definitions (1, 6) of moments gives identities.

III. MICROSCOPIC AND MACROSCOPIC BOUNDARY CONDITIONS

A. Distribution function at evaporating interface

At an evaporating liquid interface, some vapor particles that hit the interface condense, while those that do not condense are reflected; moreover, some particles are injected into the vapor by evaporation from the liquid. We write the distribution function directly in front of the interface as

$$f_{\text{int}} = \begin{cases} f^-, & C_n^{I\prime} \leq 0 \\ f^+, & C_n^I > 0 \end{cases}, \tag{12}$$

where f^- is the distribution of incident particles (negative velocity $C_n^{I\prime}$ normal, and relative, to the interface) and f^+ is the distribution of emitted particles (positive velocity C_n^I normal to the interface). The prime at the velocity of incident particles simplifies to distinguish between incident and emitted particles. For finding boundary conditions for moments, we shall describe the vapor by the R13 distribution function (10), i.e., we set $f^- = f_{|G26}$.

The distribution of particles leaving the interface is due to evaporating particles and the reflection of non-condensing particles back into the vapor. For the latter we follow the classical Maxwell model, which assumes that particles are either specularly reflected or thermalized and leave in a Maxwellian.[27,28]

The distribution of evaporating particles is obtained from the assumption that the liquid side of the interface is in local equilibrium,[33,40,41] and thus evaporating particles leave in a Maxwellian distribution $f_M\left(p_{\text{sat}}(\theta_L), \theta_L, C^I\right)$, where $p_{\text{sat}}(\theta_L)$ is the saturation pressure corresponding to the temperature θ_L of the liquid at the interface (see Appendix A). For thermal equilibrium, the outgoing distribution reduces to $f_{|E}^+ = f_{|G26,E} = f_M\left(p_{\text{sat}}(\theta_L), \theta_L, C\right)$.

The emitted distribution function consists of three terms describing evaporating particles, specularly reflected particles, and thermalized reflecting particles, respectively,

$$\begin{aligned} f^+ = &\, \vartheta f_M\left(p_{\text{sat}}(\theta_L), \theta_L, C^I\right) \\ &+ (1-\vartheta)(1-\chi)f_{|G26}\left(C_i^I - 2C_n^I n_i\right) \\ &+ (1-\vartheta)\chi f_M\left(\bar{p}, \theta_L, C^I\right). \end{aligned} \tag{13}$$

Here, ϑ is the evaporation/condensation probability and χ is the accommodation coefficient, defined as the probability that a reflected particle is thermalized. Note that in thermal equilibrium, where all distributions are equal to $f_M\left(p_{\text{sat}}(\theta_L), \theta_L, C^I\right)$, the distribution f^+ must also be equal to the Maxwellian. Hence, the factors in Eq. (13) must add to unity. The velocity C_i^I is the velocity of a vapor particle as seen from an observer resting with the liquid at the interface; $C_n^I = C_j^I n_j$ is the velocity normal to the interface; $C_i^I - 2C_n^I n_i$ is the specular reflection velocity (flipping of normal part) and the notation is such that $f_{|G26}\left(C_i^I - 2C_n^I n_i\right)$ denotes the distribution of specularly reflected particles. The pressure $\bar{p}$ in the Maxwellian for thermalized particles is determined from the condition that non-condensing particles must return to the vapor, which gives

$$\frac{\bar{p}}{m\sqrt{2\pi\theta_L}} = \int_{C_n^I > 0} f_{|G26} C_n^I d\mathbf{c}. \tag{14}$$

Since the Maxwellian is linear in pressure, and both Maxwellians in Eq. (13) depend on the liquid temperature, we can introduce the abbreviation

$$P^* = \vartheta p_{\text{sat}}(\theta_L) + (1-\vartheta)\chi\bar{p} \tag{15}$$

and rewrite the outgoing distribution in a more compact notation,

$$f^+ = f_M\left(P^*, \theta_L, C^I\right) + (1-\vartheta)(1-\chi)f_{|G26}\left(C_i^I - 2C_n^I n_i\right). \tag{16}$$

Continuity conditions for fluxes of moments are used to find the boundary conditions for the moments.[4,5,14,26] For a general description, we write the moments as

$$u_A = \int \Psi_A f d\mathbf{c}, \tag{17}$$

where $\Psi_A(c_k)$ denotes the moment generating tensor polynomials in c_k with a suitable multi-index A, and the flux of the moment u_A then is

$$F_{Ak} = \int \Psi_A c_k f \, d\mathbf{c}. \tag{18}$$

Only some of the fluxes must be continuous at the interface, as will be discussed further below.

B. Frames of reference

For the evaluation of interface conditions, we found it best to consider the fluxes from the viewpoint of an observer who slips with the gas along the liquid-vapor interface. For proper bookkeeping, we have to deal with three different particle velocities, which differ by the chosen frame of reference:

(a) the velocity relative to the liquid-vapor interface, which moves with velocity v_i^I (index n refers to the interface normal and indices t_α with $\alpha = 1, 2$ indicate the two tangential directions),

$$C_i^I = \left\{C_n^I, C_{t_\alpha}^I\right\}_i = c_i - v_i^I, \tag{19}$$

(b) the usual peculiar velocity of kinetic theory,[3] which is the velocity relative to the motion of the gas, which moves with velocity v_i, and

$$C_i = \{C_n, C_{t_\alpha}\}_i = c_i - v_i, \tag{20}$$

(c) the velocity for the slipping observer

$$\hat{C}_i = \left\{C_n^I, C_{t_\alpha}\right\}_i. \tag{21}$$

Evaporation velocity V_n and slip velocity V_{t_α} are defined as the relative macroscopic velocities between interface and gas,

$$V_i = \{V_n, V_{t_\alpha}\}_i = v_i - v_i^I. \tag{22}$$

With the interface normal n_i pointing into the gas, positive $V_n = V_i n_i$ implies evaporation and negative V_n implies condensation. Here, we chose the tangential velocity of the interface as the velocity of the liquid. Note, however, that in evaporation the normal velocity of the liquid differs from the normal velocity of the interface (see Appendix A).

The various particle velocities are related as

$$C_i^I = \left\{C_n^I, C_{t_\alpha}^I\right\}_i = \left\{C_n^I, C_{t_\alpha} + V_{t_\alpha}\right\}_i = \left\{\hat{C}_n, \hat{C}_{t_\alpha} + V_{t_\alpha}\right\}_i,$$

$$C_i = \{C_n, C_{t_\alpha}\}_i = \left\{C_n^I - V_n, C_{t_\alpha}\right\}_i = \left\{\hat{C}_n - V_n, \hat{C}_{t_\alpha}\right\}_i,$$

$$\hat{C}_i = \left\{\hat{C}_n, \hat{C}_{t_\alpha}\right\}_i = \left\{C_n^I, C_{t_\alpha}\right\}_i = \left\{C_n^I, C_{t_\alpha}^I - V_{t_\alpha}\right\}_i.$$

(23)

C. Macroscopic boundary conditions

For an observer slipping with the gas along the liquid-vapor interface, who observes the particle velocity $\hat{C}_i$, the normal flux $F_{Ak}n_k$ (18) of a moment computed with the distribution function directly at the interface, i.e., the distribution f_{int} of Eq. (12), must be equal to the normal flux computed with the distribution function $f_{|R13}$ of the gas just in front of the interface,[3] that is,

$$\int \hat{\Psi}_A \hat{C}_n f_{\text{int}} \, d\mathbf{c} = \int \hat{\Psi}_A \hat{C}_n f_{|G26} \, d\mathbf{c}$$

(24)

or, since in Eq. (12) we substitute $f^- = f_{|G26}$,

$$\int_{\hat{C}_n > 0} \hat{\Psi}_A \hat{C}_n f^+ \, d\mathbf{c} = \int_{\hat{C}_n > 0} \hat{\Psi}_A \hat{C}_n f_{|G26} \, d\mathbf{c}.$$

(25)

Here, following the work of Grad,[14] we have to use continuity only of those fluxes that are odd in $\hat{C}_n$, which implies functions $\hat{\Psi}_A$ which are even in $\hat{C}_n$. The 13 variables of the R13 equations are moments based on the weights,

$$\phi_A = m \left\{1, c_i, c^2, c_i c_j, c^2 c_i\right\}_A,$$

(26)

and of these the following tensor components are even in the normal velocity c_n:

$$\phi_{A,\text{even}} = m \left\{1, c_{t_\alpha}, c^2, c_n^2, c_{t_\alpha} c_{t_\beta}, c^2 c_{t_\alpha}\right\}_A.$$

(27)

For the observer slipping at the liquid interface, this translates into

$$\hat{\Psi}_A = m \left\{1, \hat{C}_{t_\alpha}, \hat{C}^2, \hat{C}_n^2, \hat{C}_{t_\alpha} \hat{C}_{t_\beta}, \hat{C}^2 \hat{C}_{t_\alpha}\right\}_A,$$

(28)

which must be inserted into Eq. (25). We also insert f^+ from Eq. (13) and substitute $(\hat{C}_n \mapsto -\hat{C}_n)$ in the second integral to find after some straightforward manipulations the interface conditions read (recall that $\hat{\Psi}_A$ is even in $\hat{C}_n$),

$$\int_{\hat{C}_n > 0} \hat{\Psi}_A \hat{C}_n f_M\left(P^*, \theta_L, C^L\right) \, d\mathbf{c} - [\chi + \vartheta(1-\chi)] \int_{\hat{C}_n > 0} \hat{\Psi}_A \hat{C}_n f_{|G26} d\mathbf{c} = (1-\vartheta)(1-\chi) \int \hat{\Psi}_A \hat{C}_n f_{|G26} d\mathbf{c},$$

(29)

where P^* is given by Eqs. (14) and (15).

Since all distributions are Gaussians time polynomials, the actual evaluation of the boundary conditions is straightforward, but somewhat cumbersome. Some care has to be taken to use the proper velocities for evaluation. For instance, the Maxwellian of evaporating and thermalizing particles is centered in the restframe of the liquid-vapor interface. For the evaluation, we have to consider that $\hat{C}_n = C_n^I$ and $\hat{C}_{t_\alpha} = C_{t_\alpha}^I - V_{t_\alpha}$ so that

$$\hat{\Psi}_A = m \left\{ \begin{array}{c} 1, C_{t_\alpha}^I - V_{t_\alpha}, \left(C^I\right)^2 - 2 C_{t_\alpha}^I V_{t_\alpha} + V_{t_\alpha}^2, \hat{C}_n^2, \\ \left(C_{t_\alpha}^I - V_{t_\alpha}\right)\left(C_{t_\beta}^I - V_{t_\beta}\right), \left(\left(C^I\right)^2 - 2 C_{t_\alpha}^I V_{t_\alpha} + V_{t_\alpha} V_{t_\alpha}\right)\left(C_{t_\alpha}^I - V_{t_\alpha}\right) \end{array} \right\}_A.$$

(30)

To proceed, we collect results for the relevant integrals. For the Maxwellian half-space integrals, we find

$$\int_{C_n^I > 0} \hat{\Psi}_A \hat{C}_n f_M\left(P^*, \theta_L, C^L\right) \, d\mathbf{c} = \begin{bmatrix} \frac{1}{2} P^* \sqrt{\frac{2}{\pi \theta_L}} \\ -\frac{1}{2} P^* \sqrt{\frac{2}{\pi \theta_L}} V_{t_\alpha} \\ \frac{1}{2} P^* \sqrt{\frac{2}{\pi \theta_L}} \left(4\theta_L + V_t^2\right) \\ \frac{1}{2} P^* \sqrt{\frac{2}{\pi \theta_L}} 2\theta_L \\ \frac{1}{2} P^* \sqrt{\frac{2}{\pi \theta_L}} \left(\theta_L \delta_{\alpha\beta} + V_{t_\alpha} V_{t_\beta}\right) \\ -\frac{1}{2} P^* \sqrt{\frac{2}{\pi \theta_L}} V_{t_\alpha} \left(6\theta_L + V_{t_\beta} V_{t_\beta}\right) \end{bmatrix}_A.$$

(31)

For the other integrals in Eq. (29), we have to re-write the distribution function $f_{|R13}$ (10) for the slipping observer, i.e., with the velocity $\hat{C}_i$. To make the procedure manageable, we consider only linear effects in non-equilibrium. For this we insert $C_i = \left\{\hat{C}_n - V_n, \hat{C}_{t_\alpha}\right\}_i$ into Eq. (10) and expand to linear terms in all non-equilibrium quantities $\left\{V_n, \Delta, q_k, \sigma_{ij}, R_{ij}, m_{ijk}\right\}$. In particular, this restricts the results to evaporation velocities V_n well below the speed of sound. With this restriction, we find

$$f_{|G26}\left(\hat{C}_i\right) = \frac{\rho}{m} \frac{1}{(2\pi\theta)^{3/2}} \exp\left(-\frac{\hat{C}^2}{2\theta}\right)\left(1 + \frac{V_n}{\theta}\hat{C}_n + \frac{\Delta}{120\rho\theta^4}\left(15\theta^2 - 10\theta\hat{C}^2 + \hat{C}^4\right)\right.$$

$$\left. + \frac{1}{5}\frac{q_k}{\rho\theta^3}\hat{C}_k\left(\hat{C}^2 - 5\theta\right) + \frac{\sigma_{ij}}{2\rho\theta^2}\hat{C}_{\langle i}\hat{C}_{j\rangle} - \frac{R_{ij}}{28\rho\theta^4}\hat{C}_{\langle i}\hat{C}_{j\rangle}\left(7\theta - \hat{C}^2\right) + \frac{m_{ijk}}{6\rho\theta^3}\hat{C}_{\langle i}\hat{C}_j\hat{C}_{k\rangle}\right).$$

(32)

From this, the full fluxes of $f_{|G26}$ are calculated as

$$
\int \hat{\Psi}_A \hat{C}_n f_{|G26}\, d\mathbf{c} =
\begin{bmatrix}
\rho V_n \\[6pt]
\sigma_{t_\alpha n} \\[6pt]
2\left(q_n + \dfrac{5}{2}\rho\theta V_n\right) \\[6pt]
m_{nnn} + \dfrac{6}{5}\left(q_n + \dfrac{5}{2}\rho\theta V_n\right) \\[6pt]
m_{t_\alpha t_\beta n} + \dfrac{2}{5}\left(q_n + \dfrac{5}{2}\rho\theta V_n\right)\delta_{\alpha\beta} \\[6pt]
R_{t_\alpha n} + 7\theta\sigma_{t_\alpha n}
\end{bmatrix}_A
\tag{33}
$$

and the corresponding half fluxes as

$$
\int_{\hat{C}_n>0} \hat{\Psi}_A \hat{C}_n f_{|G26}\, d\mathbf{c} =
\begin{bmatrix}
\dfrac{1}{2}\rho V_n + \dfrac{1}{2}\sqrt{\dfrac{2}{\pi\theta}}\,\Pi \\[8pt]
\dfrac{\sigma_{t_\alpha n}}{2} + \sqrt{\dfrac{2}{\pi\theta}}\left(\dfrac{1}{4}m_{t_\alpha nn} + \dfrac{1}{10}q_{t_\alpha}\right) \\[8pt]
q_n + \dfrac{5}{2}\rho\theta V_n + \sqrt{\dfrac{2}{\pi\theta}}\left(2\Pi\theta + \dfrac{1}{2}\theta\sigma_{nn} + \dfrac{\Delta}{15} + \dfrac{5}{28}R_{nn}\right) \\[8pt]
\dfrac{1}{2}m_{nnn} + \dfrac{3}{5}\left(q_n + \dfrac{5}{2}\rho\theta V_n\right) + \sqrt{\dfrac{2}{\pi\theta}}\left(\Pi\theta + \theta\sigma_{nn} + \dfrac{1}{7}R_{nn} + \dfrac{1}{30}\Delta\right) \\[8pt]
\begin{bmatrix}
\dfrac{1}{2}m_{t_\alpha t_\beta n} + \dfrac{1}{5}\left(q_n + \dfrac{5}{2}\rho\theta V_n\right)\delta_{\alpha\beta} \\[6pt]
+\sqrt{\dfrac{2}{\pi\theta}}\left(\dfrac{\theta}{2}\sigma_{t_\alpha t_\beta} + \dfrac{R_{t_\alpha t_\beta}}{28} + \left(\dfrac{1}{2}\Pi\theta + \dfrac{\Delta}{60} + \dfrac{R_{nn}}{28}\right)\delta_{\alpha\beta}\right)
\end{bmatrix} \\[8pt]
\dfrac{1}{2}\left(R_{t_\alpha n} + 7\theta\sigma_{t_\alpha n}\right) + \sqrt{\dfrac{2}{\pi\theta}}\left(2\theta m_{t_\alpha nn} + \dfrac{9}{5}\theta q_{t_\alpha}\right)
\end{bmatrix}.
\tag{34}
$$

Here, we have introduced the effective pressure Π as

$$
\Pi = \rho\theta + \frac{1}{2}\sigma_{nn} - \frac{1}{120}\frac{\Delta}{\theta} - \frac{1}{28}\frac{R_{nn}}{\theta}.
\tag{35}
$$

D. Evaporation boundary conditions for R13

The integrals of Sec. III C are all that is required to find the boundary conditions for the R13 equations at evaporating and condensing interfaces by the evaluation of Eq. (29). Before we list the results, we point out the deficiency of the R13 equations to fully resolve Knudsen layers, which was discussed, e.g., in Ref. 42. Indeed, full resolution of the Knudsen layer requires a larger number of moments, which is not feasible in practice.[22,43] However, solutions of the R13 equations between solid walls, i.e., no evaporation or condensation, have shown that their ability not only to describe jump and slip at the boundaries but also to approximate Knudsen layers leads to a marked improvement of the overall simulation.

The usual way to improve the boundary conditions is to introduce correction coefficients for jump and slip into the interface conditions, which is usually done in jump and slip hydrodynamics.[7,26] A more careful approach to correct the boundary conditions for R13 equations uses the ideas of thermodynamics of irreversible processes[44,45] to derive interface conditions with tunable Onsager coefficients from the entropy generation at the interface, based on the R13

approximation of the entropy flux.[42] A similar approach could be useful for the evaporation case, but this is deferred to future work.

The expression for the evaporation mass flux results for $\hat{\Psi}_A = 1$ as

$$
\rho V_n = \frac{\vartheta}{2-\vartheta}\sqrt{\frac{2}{\pi}}\left(\frac{p_{\text{sat}}(\theta_L)}{\sqrt{\theta_L}} - \frac{\Pi}{\sqrt{\theta}}\right).
\tag{36}
$$

Hence, the evaporation flux is determined through the difference between the saturation pressure $p_{\text{sat}}(\theta_L)$ of the liquid at the interface (weighted with the factor $\sqrt{\frac{\theta}{\theta_L}}$) and the effective pressure Π. This expression is a generalization of the classical Hertz-Knudsen-Schrage law[46–49] to the R13 equations. For non-evaporating surfaces, where $\vartheta = 0$, this reduces to the statement that there is no flow through the surface, $V_n = 0$. The classical Hertz-Knudsen law replaces Π with the pressure p of the vapor and replaces the factor $\sqrt{2/\pi}$ by $1/\sqrt{2\pi}$. The correction of the latter factor due to Schrage accounts for the fact that the vapor is in a non-equilibrium state, as it is in the R13 equations.

The other conditions are generalizations of the established wall boundary conditions for the R13 equations,[26] to which they reduce for non-evaporating interfaces ($\vartheta = 0$). Due to the evaporation and condensation processes, there are additional contributions with the evaporation flux ρV_n, and the evaporation coefficient appears in the overall slip and

jump coefficients $\frac{\vartheta + \chi(1-\vartheta)}{2-\vartheta-\chi(1-\vartheta)}$ (which for $\vartheta = 0$ reduces to the familiar form $\frac{\chi}{2-\chi}$). The conditions for $m_{t_\alpha t_\beta n}$ and $R_{t_\alpha n}$ are extensions to two-tangential directions, which were not stated in the literature before so that the interface conditions below allow us to formulate three dimensional problems.

In summary, we find the following interface relations:
Generalized velocity slip condition,

$$
\sigma_{t_\alpha n} = -\frac{\vartheta + \chi(1-\vartheta)}{2-\vartheta-\chi(1-\vartheta)}\sqrt{\frac{2}{\pi\theta}}
$$
$$
\times \left(\Pi V_{t_\alpha} + \frac{1}{5}q_{t_\alpha} + \frac{1}{2}m_{t_\alpha nn} \right) - \rho V_n V_{t_\alpha}, \quad (37)
$$

generalized temperature jump condition,

$$
q_n = -\frac{\vartheta + \chi(1-\vartheta)}{2-\vartheta-\chi(1-\vartheta)}\sqrt{\frac{2}{\pi\theta}}
$$
$$
\times \left(2\Pi(\theta-\theta_L) - \frac{\Pi}{2}V_t^2 + \frac{1}{2}\theta\sigma_{nn} + \frac{\Delta}{15} + \frac{5}{28}R_{nn} \right)
$$
$$
+ \left[\frac{1}{2}\left(V_t^2 - \theta_L\right) - \frac{5}{2}(\theta-\theta_L) \right]\rho V_n, \quad (38)
$$

generalized interface conditions for higher moments,

$$
m_{nnn} = \frac{\vartheta + \chi(1-\vartheta)}{2-\vartheta-\chi(1-\vartheta)}\sqrt{\frac{2}{\pi\theta}}
$$
$$
\times \left[\frac{2}{5}\Pi(\theta-\theta_L) - \frac{3}{5}\Pi V_t^2 - \frac{7}{5}\theta\sigma_{nn} \right.
$$
$$
\left. + \frac{\Delta}{75} - \frac{1}{14}R_{nn} \right] - \frac{2}{5}\left[\theta_L + \frac{3}{2}V_t^2 \right]\rho V_n, \quad (39)
$$

$$
m_{t_\alpha t_\beta n} = -\frac{\vartheta + \chi(1-\vartheta)}{2-\vartheta-\chi(1-\vartheta)}\sqrt{\frac{2}{\pi\theta}}
$$
$$
\times \left[\theta\sigma_{t_\alpha t_\beta} - \Pi V_{t_\alpha}V_{t_\beta} + \frac{R_{t_\alpha t_\beta}}{14} \right.
$$
$$
\left. + \left(\frac{1}{5}\Pi(\theta-\theta_L) + \frac{1}{5}\Pi V_t^2 - \frac{1}{5}\theta\sigma_{nn} + \frac{\Delta}{150} \right)\delta_{\alpha\beta} \right]
$$
$$
+ \rho V_n \left[V_{t_\alpha}V_{t_\beta} + \frac{1}{5}\left(\theta_L - V_t^2\right)\delta_{\alpha\beta} \right], \quad (40)
$$

$$
R_{t_\alpha n} = \frac{\vartheta + \chi(1-\vartheta)}{2-\vartheta-\chi(1-\vartheta)}\sqrt{\frac{2}{\pi\theta}}
$$
$$
\times \left[\Pi\theta V_{t_\alpha} - \frac{11}{5}\theta q_{t_\alpha} - \frac{1}{2}\theta m_{t_\alpha nn} \right.
$$
$$
\left. - \Pi V_{t_\alpha}V_{t_\beta}V_{t_\beta} + 6\Pi V_{t_\alpha}(\theta-\theta_L) \right]
$$
$$
+ \left[7(\theta-\theta_L) + \theta_L - V_{t_\beta}V_{t_\beta} \right]\rho V_{t_\alpha} V_n. \quad (41)
$$

In Sec. IV, we shall proceed with the evaluation of the above interface conditions and study applications to some simple evaporation problems.

E. Interface conditions for hydrodynamics

In the hydrodynamic limit, only first order contributions in the Knudsen number are retained in the equations. Analysis of the bulk transport equations by means of the order of magnitude method[12] reveals that stress σ_{ij} and heat flux q_n are of

first order in Kn and are given by the Navier-Stokes-Fourier equations (5), while m_{ijk}, Δ, and R_{ij} are of second order. The evaporation mass flux ρV_n is not linked to the Knudsen number, but we have already considered it to be small of first order in all equations. Thus, for the hydrodynamic limit, we consider only terms linear in V_n, V_{t_α}, σ_{ij}, and q_i in the above, to obtain the interface conditions for hydrodynamics which are as follows:

(a) evaporation/condensation mass flow,

$$
[\rho V_n]_{|NSF} = \frac{\vartheta}{2-\vartheta}\sqrt{\frac{2}{\pi}}\left(\frac{p_{sat}(\theta_L)}{\sqrt{\theta_L}} - \frac{p}{\sqrt{\theta}} - \frac{\sigma_{nn}}{2\sqrt{\theta}} \right),
$$
$$
(42)
$$

(b) slip condition, and

$$
[\sigma_{t_\alpha n}]_{|NSF} = -\frac{\vartheta + \chi(1-\vartheta)}{2-\vartheta-\chi(1-\vartheta)}\sqrt{\frac{2}{\pi\theta}}\left(pV_{t_\alpha} + \frac{1}{5}q_{t_\alpha} \right),
$$
$$
(43)
$$

(c) evaporation/condensation heat transfer,

$$
[q_n]_{|NSF} = -\frac{\vartheta + \chi(1-\vartheta)}{2-\vartheta-\chi(1-\vartheta)}\sqrt{\frac{2}{\pi\theta}}
$$
$$
\times \left(2\Pi(\theta-\theta_L) - \frac{\rho\theta}{2}V_t^2 + \frac{1}{2}\theta\sigma_{nn} \right)
$$
$$
+ \left[\frac{1}{2}\left(V_t^2 - \theta_L\right) - \frac{5}{2}(\theta-\theta_L) \right]\rho V_n.
$$
$$
(44)
$$

The subscript NSF indicates that these are the appropriate boundary conditions for classical hydrodynamics. It is implied, of course, that in the above, stress tensor and heat flux are given by the laws of Navier-Stokes and Fourier (5). The mass flux condition (42) is known as the Hertz-Knudsen-Schrage law, which is an improvement of the classical Hertz-Knudsen law to account for the effect of flow in the vapor.[46–49] The slip condition (43) is the typical slip condition for a gas,[7] only that the overall slip coefficient now depends on the evaporation coefficient ϑ as well. Typically, the contribution with σ_{nn} in Eq. (42) does not appear in the literature, since it vanishes for NSF in planar geometry, as, e.g., in the problems below. It should be included, however, since it will contribute for curved phase interfaces, such as in droplets and bubbles.

Quite often in the discussion of evaporation mass flows, a condition for energy flux (44) is not given. It is clear, however, that the simulation of an evaporation experiment requires the full set of transport equations with the appropriate boundary conditions; hence, an interface condition for energy flux (and possibly higher moments) is necessary. We point to our earlier work[49] where an evaporation experiment was evaluated with a variant of the Schrage model, and it became clear that the evaporation flow was mainly determined by the amount of heat transferred to the interface through the liquid, while the mass flow condition determined the liquid temperature, and the heat flux condition determined the temperature jump between liquid and vapor at the interface.

For one-dimensional processes in planar geometry, with transport only normal to the interface, and for only small deviations from equilibrium, Eqs. (42) and (44) reduce to

$$[\rho V_n]_{|\text{NSF}} = \frac{2\vartheta}{2-\vartheta}\left(\frac{p_{\text{sat}}(\theta_L) - p}{\sqrt{2\pi\theta_L}} - \frac{1}{2}\frac{p}{\sqrt{2\pi\theta_L}}\frac{\theta_L - \theta}{\theta_L}\right),$$
(45)

$$\frac{[q_n]_{|\text{NSF}}}{\theta_L} = 4\frac{\vartheta + \chi(1-\vartheta)}{2-\vartheta-\chi(1-\vartheta)}\frac{p}{\sqrt{2\pi\theta_L}}\frac{(\theta_L - \theta)}{\theta_L} - \frac{1}{2}\rho V_n.$$
(46)

The above can be rewritten as

$$\begin{bmatrix} [\rho V_n]_{|\text{NSF}} \\ \dfrac{[q_n]_{\text{NSF}}}{\theta_L} \end{bmatrix} = \begin{bmatrix} \dfrac{2\vartheta}{2-\vartheta} & -\dfrac{\vartheta}{2-\vartheta} \\ -\dfrac{\vartheta}{2-\vartheta} & \left[\dfrac{4\vartheta+4\chi(1-\vartheta)}{2-\vartheta-\chi(1-\vartheta)} + \dfrac{1}{2}\dfrac{\vartheta}{2-\vartheta}\right] \end{bmatrix}$$
$$\times \begin{bmatrix} \dfrac{p_{\text{sat}}(\theta_L) - p}{\sqrt{2\pi\theta_L}} \\ \dfrac{p}{\sqrt{2\pi\theta_L}}\dfrac{\theta_L - \theta}{\theta_L} \end{bmatrix},$$
(47)

which is the natural form in the theory of linear irreversible thermodynamics[28,50] with a symmetric matrix of Onsager coefficients.

Further reduction by assuming full accommodation ($\chi = 1$) and inversion of the matrix gives

$$\begin{bmatrix} \dfrac{p_{\text{sat}}(\theta_L) - p}{\sqrt{2\pi\theta_L}} \\ \dfrac{p}{\sqrt{2\pi\theta_L}}\dfrac{\theta_L - \theta}{\theta_L} \end{bmatrix} = \begin{bmatrix} \hat{r}_{11} & \hat{r}_{12} \\ \hat{r}_{12} & \hat{r}_{22} \end{bmatrix}\begin{bmatrix} [\rho V_n]_{|\text{NSF}} \\ \dfrac{[q_n]_{\text{NSF}}}{\theta_L} \end{bmatrix}$$
(48)

with the symmetric matrix of resistivities[28]

$$\hat{r}_{\alpha\beta} = \begin{bmatrix} \left(\dfrac{1}{\vartheta} - \dfrac{1}{2}\right) + \dfrac{1}{16} & \dfrac{1}{8} \\ \dfrac{1}{8} & \dfrac{1}{4} \end{bmatrix}_{\alpha\beta}.$$
(49)

Exact calculations based on kinetic theory (with full accommodation, $\chi = 1$) yield explicit corrections to account for Knudsen layer effects[33,50] with the resistivities

$$\hat{r}_{\alpha\beta|\text{corr}} = \begin{bmatrix} \dfrac{1}{\vartheta} + \dfrac{1}{\pi} - \dfrac{23}{32} & \dfrac{1}{16} + \dfrac{1}{5\pi} \\ \dfrac{1}{16} + \dfrac{1}{5\pi} & \dfrac{1}{8} + \dfrac{13}{25\pi} \end{bmatrix}_{\alpha\beta}$$
$$= \begin{bmatrix} \dfrac{1}{\vartheta} - 0.400\,44 & 0.126 \\ 0.126 & 0.291 \end{bmatrix}_{\alpha\beta}.$$
(50)

We shall examine both sets of resistivities in the examples below.

IV. 1-D HEAT AND MASS TRANSFER PROBLEMS

A. One-dimensional equations

To put the R13 equations with evaporation/condensation to test, we now consider flows in simple one-dimensional geometry and steady state. For simplicity, we ignore all details of mass and heat transfer through the liquid and consider the temperature of the liquid at the interface as given. The normal of the interface points into the $x_1 = x$ direction, and all flow properties are functions only of this coordinate.

For these first tests, we consider small deviations from a rest state where vapor and liquid are in equilibrium at temperature θ_0, hence the reference pressure is $p_0 = p_{\text{sat}}(\theta_0) = \rho_0\theta_0$. We use the rest state data and the length scale L to make the variables dimensionless. With all flows only in the x-direction, the variable space is reduced to

$$\hat{\rho}(\hat{x}) = \frac{\rho(L\hat{x})}{\rho_0}, \quad \hat{\theta}(\hat{x}) = \frac{\theta(L\hat{x})}{\theta_0},$$

$$\hat{v}_k(\hat{x}) = \left\{\frac{v(L\hat{x})}{\sqrt{\theta_0}}, 0, 0\right\}, \quad \hat{q}_k(\hat{x}) = \left\{\frac{q(L\hat{x})}{p_0\sqrt{\theta_0}}, 0, 0\right\},$$ (51)

$$\hat{\sigma}_{ij}(\hat{x}) = \text{diag}\left[\frac{\sigma(L\hat{x})}{p_0}, -\frac{1}{2}\frac{\sigma(L\hat{x})}{p_0}, -\frac{1}{2}\frac{\sigma(L\hat{x})}{p_0}\right]_{ij}.$$

We simplify the R13 equations (2)–(4) and (8) for geometry, keeping only first order terms in the velocity. The linearized dimensionless conservation laws (2) become (for a simpler notation, we omit the circumflexes that indicate dimensionless quantities)

$$\frac{\partial}{\partial x}(\rho v) = \frac{\partial}{\partial x}(p + \sigma) = \frac{\partial}{\partial x}\left(\frac{5}{2}\rho v\theta + q\right) = 0,$$ (52)

which are easily integrated to give constant mass flow J_0, constant normal stress P_0, and constant overall energy flux Q_0,

$$\rho v = J_0 = const., \quad p + \sigma = P_0 = const.,$$
$$\frac{5}{2}J_0\theta + q = Q_0 = const.$$ (53)

With this, the (linearized, dimensionless, one-dimensional) R13 constitutive equations for Maxwell molecules (8) or the BGK model (9) reduce to

$$\Delta = -\frac{12}{\beta}\text{Kn}\frac{\partial q}{\partial x} = \frac{30}{\beta}\text{Kn}J_0\frac{\partial\theta}{\partial x} \simeq 0,$$
$$R = -\frac{16}{5}\gamma\text{Kn}\frac{\partial q}{\partial x} = 8\gamma\text{Kn}J_0\frac{\partial q}{\partial x} \simeq 0,$$ (54)
$$m = -\frac{6\beta}{5}\text{Kn}\frac{\partial\sigma}{\partial x},$$

where the coefficients β, γ distinguish between Maxwell molecules ($\beta_{\text{MM}} = \gamma_{\text{MM}} = 1$) and the BGK model ($\beta_{\text{BGK}} = \frac{3}{2}$, $\gamma_{\text{BGK}} = \frac{7}{6}$). Note that, due to linearization, products such as $J_0\frac{\partial\theta}{\partial x}$ and $J_0\frac{\partial\sigma}{\partial x}$ can be ignored.

The linearized balance equations for the xx-component of stress (3) and the x-component of heat flux (4) reduce to (with $q_0 = Q_0 - \frac{5}{2}J_0$)

$$\frac{6\beta}{5}\text{Kn}\frac{\partial^2\sigma}{\partial x^2} = \frac{\sigma}{\text{Kn}}, \quad \frac{\partial\theta}{\partial x} = -\frac{4\beta q_0}{15\text{Kn}} - \frac{2}{5}\frac{\partial\sigma}{\partial x}.$$ (55)

These can be integrated easily to give

$$\theta = K - \frac{4\beta q_0 x}{15\text{Kn}} - \frac{2}{5}\sigma,$$
$$\sigma = A\sinh\left[\sqrt{\frac{5}{6\beta}}\frac{x}{\text{Kn}}\right] + B\cosh\left[\sqrt{\frac{5}{6\beta}}\frac{x}{\text{Kn}}\right],$$ (56)

where K, A, B are constants of integration. We note that σ is of the Knudsen layer type, i.e., it decays exponentially away from the interface on the scale of the mean free path. We also note

that classical hydrodynamics gives $\sigma = 0$, and $\theta = K - \frac{4q_0 x}{15\text{Kn}}$, which is the case for $A = B = 0$.

For the full solution, we have to find the 6 constants of integration $\{J_0, P_0, q_0, K, A, B\}$, which requires 6 boundary conditions in total, that is, 3 boundary conditions on either side of the domain.

When a boundary is a liquid-vapor interface, we will use the appropriate boundary conditions from (36)–(41) which in linearized and dimensionless form reduce to (no tangential components)

$$J_{0,n} = \frac{\vartheta}{2 - \vartheta} \sqrt{\frac{2}{\pi}} \left(p_{\text{sat}}(\theta_L) - P_0 - \frac{1}{2}(\theta_L - \theta) + \frac{1}{2}\sigma \right),$$

$$q_{0,n} = \frac{\vartheta + \chi(1 - \vartheta)}{2 - \vartheta - \chi(1 - \vartheta)} \sqrt{\frac{2}{\pi}} \left(2(\theta_L - \theta) - \frac{1}{2}\sigma \right) - \frac{1}{2}J_{0,n},$$

$$\frac{6\beta}{5}\text{Kn} \left[\frac{\partial \sigma}{\partial x} \right]_n = \frac{\vartheta + \chi(1 - \vartheta)}{2 - \vartheta - \chi(1 - \vartheta)} \sqrt{\frac{2}{\pi}}$$
$$\times \left[\frac{2}{5}(\theta_L - \theta) + \frac{7}{5}\sigma \right] + \frac{2}{5}J_{0,n}. \quad (57)$$

Here it is assumed that all dimensionless pressures $p_{\text{sat}}(\theta_L)$, P_0, and all dimensionless temperatures θ_L, θ, are close to unity. $J_{0,n}, q_{0,n}$ are the products of the flows J_0, q_0 with the normal at the respective boundary.

For NSF, we consider the interface conditions (48), either with the simple resistivities (49) or with the corrected resistivities (50), which we write for easy comparison with the above as

$$J_{0,n} = \frac{\hat{r}_{22}/2}{\hat{r}_{11}\hat{r}_{22} - \hat{r}_{12}\hat{r}_{12}} \sqrt{\frac{2}{\pi}} \left(p_{\text{sat}}(\theta_L) - P_0 - \frac{\hat{r}_{12}}{\hat{r}_{22}}(\theta_L - \theta) \right),$$

$$q_{0,n} = \frac{1}{4\hat{r}_{22}} \sqrt{\frac{2}{\pi}} (2(\theta_L - \theta)) - \frac{\hat{r}_{12}}{\hat{r}_{22}} V_n. \quad (58)$$

Since we only consider the temperature of the liquid at the interface, but not the detailed transport processes through the liquid layers, the relations for these given in Appendix A are not required.

B. Half-space problem

We first consider the classical problem of the steady evaporation into a half-space, consisting of an evaporating interface at temperature θ_L with evaporation pressure $p_{\text{sat}}(\theta_L)$ where evaporation is forced by prescribing the pressure $p_\infty = P_0$ at a large distance of the interface. Dimensionless temperature θ_∞ and velocity $v_\infty = J_0$ are controlled such that the vapor at a large distance is in a drifting equilibrium state.

A comprehensive account of the kinetic theory treatment of the problem is given in Ref. 30. Here, we compare the R13 solution with Pao's results from the linearized BGK model[31] and with the linearized form of non-linear jump formulas derived by Ytrehus by a moment method solution of the Boltzmann equation for Maxwell molecules.[29] Both formulations assume perfect evaporation ($\vartheta = 1$).

The conditions for this problem require $q_0 = \sigma_\infty = 0$ and hence the solution of the problem follows from Eq. (56) as

$$\theta(x) = \theta_\infty - \frac{2}{5}\sigma(x), \quad \sigma(x) = A \exp\left[-\sqrt{\frac{5}{6\beta}} \frac{x}{\text{Kn}} \right]. \quad (59)$$

With the pressure p_∞ prescribed, the unknowns of the problem are temperature θ_∞, evaporation speed v_∞, and the constant A for the normal stress. These follow from the boundary conditions at the interface (57), which for this problem can be brought into the form

$$v_\infty = \frac{\vartheta}{2 - \vartheta} \sqrt{\frac{2}{\pi}} \left(p_{\text{sat}}(\theta_L) - p_\infty - \frac{1}{2}(\theta_L - \theta_\infty) + \frac{3}{10}A \right),$$

$$v_\infty = \frac{\vartheta + \chi(1 - \vartheta)}{2 - \vartheta - \chi(1 - \vartheta)} \sqrt{\frac{2}{\pi}} \left(4(\theta_L - \theta_\infty) + \frac{3}{5}A \right),$$

$$v_\infty = -\frac{\vartheta + \chi(1 - \vartheta)}{2 - \vartheta - \chi(1 - \vartheta)} \sqrt{\frac{2}{\pi}} \left[\theta_L - \theta_\infty + \frac{39}{10}A \right] - \sqrt{\frac{15\beta}{2}}A. \quad (60)$$

For hydrodynamics, the corresponding equations based on (58) must be used, with the resistivities (49) or (50); after linearization,

$$v_\infty = \frac{p_{\text{sat}}(\theta_L) - p_\infty}{\sqrt{2\pi}\hat{r}_{11}}, \quad v_\infty = \frac{1}{\sqrt{2\pi}} \frac{\theta_L - \theta}{\hat{r}_{21}}. \quad (61)$$

For comparison of the various models, we follow the work of Ytrehus and consider the dimensionless ratios

$$\alpha_p = \frac{p_{\text{sat}}(\theta_L^0) - p^\infty}{v_\infty/\sqrt{2}}, \quad \alpha_\theta = \frac{\theta_L - \theta_\infty}{v_\infty/\sqrt{2}}, \quad (62)$$

which are just the resistivities $\hat{r}_{11}$ and $\hat{r}_{12}$ of Eq. (48) multiplied by $2\sqrt{\pi}$. We compare results from R13, Ytrehus (Y), Pao (P), and hydrodynamics [NSF and corr.NSF, with the coefficients (49) or (50), respectively], for which we find

$$\alpha_{p|\text{NSF}} = \alpha_{p|\text{P}} = 2\sqrt{\pi}\hat{r}_{11} = \frac{9}{8}\sqrt{\pi} = 1.994\,01,$$

$$\alpha_{p|\text{Y}} = \alpha_{p|\text{corr.NSF}} = \frac{9}{16}\sqrt{\pi} + \frac{2}{\sqrt{\pi}} = 2.125\,38, \quad (63)$$

$$\alpha_{p|\text{R13}} = \frac{75\sqrt{\pi} + 9\pi\sqrt{15\beta}}{60 + 8\sqrt{15\pi\beta}} = \begin{cases} 2.109\,69 & (\beta = 1) \\ 2.098\,47 & (\beta = 3/2) \end{cases}$$

and

$$\alpha_{\theta|\text{Y}} = \alpha_{\theta|\text{P}} = \frac{\sqrt{\pi}}{4} = 0.443\,113,$$

$$\alpha_{\theta|\text{NSF}} = 2\sqrt{\pi}\hat{r}_{12} = \frac{\sqrt{\pi}}{4} = 0.443\,113,$$

$$\alpha_{\theta|\text{corr.NSF}} = 2\sqrt{\pi}\hat{r}_{12} = 2\sqrt{\pi}\left(\frac{1}{16} + \frac{1}{5\pi} \right) = 0.447\,23,$$

$$\alpha_{\theta|\text{R13}} = \frac{\sqrt{\pi}\left(9 + \sqrt{15\pi\beta} \right)}{30 + 4\sqrt{15\pi\beta}} = \begin{cases} 0.489\,385 & (\beta = 1) \\ 0.484\,897 & (\beta = 3/2) \end{cases}. \quad (64)$$

The corrected NSF values (corr.NSF) agree with the exact data, since they were fitted to similar results. Pao's results agree with our NSF results (49), that is, without any Knudsen layer correction.

For this problem, the R13 equations for Maxwell molecules ($\beta = 1$) and the BGK model ($\beta = 3/2$) give almost identical results. The coefficient α_p agrees well with Ytrehus' result (relative error 0.7%), which in turn agrees well with our own numerical solution for the BGK model. For the temperature coefficient α_θ, however, the R13 equations differ from the accurate value (also confirmed by numerical solution of BGK) by about 10%. This deviation is similar to the deviation of temperature jump and slip for the R13 equation in half-space problems which was pointed out in Ref. 51 and discussed in detail in Ref. 42.

The results presented next will show that for larger Knudsen numbers, all macroscopic models cannot accurately model heat flux *and* temperature profile simultaneously. The coefficient α_θ is extracted from the temperature profile, that is, its deviation is related to this conflict.

To close this section, we point out that in this particular half-space problem, the non-convective heat flux, q, vanishes, which implies that the boundary conditions cannot be fully explored. This is evident from the observation that the resistivity $\hat{r}_{22}$ of Eq. (48) does not occur in the solution for the NSF problem.

C. Heat and mass transfer between two reservoirs

Next we study heat and mass transfer between two liquid reservoirs (see Fig. 1), comparing predictions of macroscopic equations (NSF, R13) with Direct Simulation Monte Carlo (DSMC) results. This problem is richer than the previous one, in that it has a non-vanishing heat flux. Also, we will look at detailed profiles, including resolved Knudsen layers, of temperature and normal stress.

To be specific, we consider one-dimensional transport between two liquid layers identified with sub- or super-scripts 0, 1 located at (dimensionless) locations $x_{0,1} = \mp\frac{1}{2}$. For the solution, we have to consider boundary conditions on both sides of the domain. The interface normal points into the vapor, i.e., into the positive direction at $x_0 = -\frac{1}{2}$ and into the negative direction at $x_1 = \frac{1}{2}$; accordingly $V_n(x_1) = -V_n(x_0) = -J_0$, etc. We need to consider the boundary conditions (57) at both boundaries. The three pairs (57) of boundary conditions for V_n, q_n, m_{nnn} are best applied by taking their pairwise sums and differences, respectively. After some calculation, the solution of the linear problems (53) and (56) assumes the form
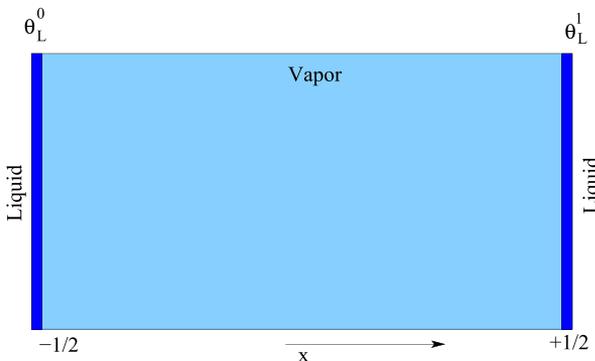

FIG. 1. Setup for heat and mass transfer between two reservoirs.

$$P_0 = \frac{p_{\text{sat}}\left(\theta_L^0\right) + p_{\text{sat}}\left(\theta_L^1\right)}{2},$$

$$\theta = \frac{\theta_L^0 + \theta_L^1}{2} - \frac{4\beta q_0}{15\text{Kn}}x - \frac{2}{5}A\sinh\left[\sqrt{\frac{5}{6\beta}}\frac{x}{\text{Kn}}\right], \quad (65)$$

$$\sigma = A\sinh\left[\sqrt{\frac{5}{4\beta}}\frac{x}{\text{Kn}}\right].$$

Two of the pairwise sums of the BC give $\left(\theta_L^0 - \theta^0\right) + \left(\theta_L^1 - \theta^1\right) = 0$, which was used to simplify the above.

The evaporation fluxes J_0, the heat flux q_0, and the amplitude of the Knudsen layer A are obtained from a linear system which results from subtracting the interface conditions at both sides,

$$J_0 = \frac{\vartheta}{2-\vartheta}\sqrt{\frac{2}{\pi}}\frac{1}{2}\left(p_{\text{sat}}\left(\theta_L^0\right) - p_{\text{sat}}\left(\theta_L^1\right)\right)$$
$$+ \frac{1}{2}\left(\frac{4\beta q_0}{15\text{Kn}} + \theta_L^1 - \theta_L^0\right) - \frac{3}{5}A\sinh\left[\sqrt{\frac{5}{6\beta}}\frac{1}{2\text{Kn}}\right]\right),$$

$$q_0 = -\frac{\vartheta + \chi(1-\vartheta)}{2-\vartheta-\chi(1-\vartheta)}\sqrt{\frac{2}{\pi}}\left(\frac{4\beta q_0}{15\text{Kn}} + \theta_L^1 - \theta_L^0\right.$$
$$\left. + \frac{3}{10}A\sinh\left[\sqrt{\frac{5}{6\beta}}\frac{1}{2\text{Kn}}\right]\right) - \frac{J_0}{2}, \quad (66)$$

$$\sqrt{30\beta}A\cosh\left[\sqrt{\frac{5}{6\beta}}\frac{1}{2\text{K n}}\right] = -\frac{\vartheta + \chi(1-\vartheta)}{2-\vartheta-\chi(1-\vartheta)}\sqrt{\frac{2}{\pi}}$$
$$\times\left[\frac{4\beta q_0}{15\text{Kn}} + \theta_L^1 - \theta_L^0\right.$$
$$\left. + \frac{39}{5}A\sinh\left[\sqrt{\frac{5}{6\beta}}\frac{1}{2\text{K n}}\right]\right] + 2J_0.$$

Inversion of this system yields the integration constants $\{J_0, q_0, A\}$ and insertion of these into (65) gives detailed profiles of temperature and stress.

The NSF solution is obtained by setting $A = 0$ in Eq. (65), which implies $\sigma = 0$ so that $p = P_0$ is the homogenous pressure in the vapor. Subtraction of the interface conditions (48) on both sides yields two equations for mass and heat flux that, for comparison with the corresponding R13 expressions from above, are best written as

$$J_0 = \frac{1}{2}\frac{\hat{r}_{22}}{\hat{r}_{11}\hat{r}_{22} - \hat{r}_{12}\hat{r}_{21}}\sqrt{\frac{2}{\pi}}\frac{1}{2}\left[\hat{p}_{\text{sat}}\left(\theta_L^0\right) - \hat{p}_{\text{sat}}\left(\theta_L^1\right)\right.$$
$$\left. + \frac{\hat{r}_{12}}{\hat{r}_{22}}\left(\frac{4\beta q_0}{15\text{Kn}} + \hat{\theta}_L^1 - \hat{\theta}_L^0\right)\right], \quad (67)$$

$$q_0 = -\frac{1}{4\hat{r}_{22}}\sqrt{\frac{2}{\pi}}\left(\frac{4\beta q_0}{15\text{Kn}} + \hat{\theta}_L^1 - \hat{\theta}_L^0\right) - \frac{\hat{r}_{21}}{\hat{r}_{22}}J_0.$$

The final solution of the problem is obtained by solving (67) for J_0 and q_0 and inserting the results (with $A = 0$) into Eq. (65).

R13 and NSF results will now be compared to DSMC simulations (for $\beta = 1$), for which we set the evaporation coefficient ϑ to unity so that $\frac{\vartheta}{2-\vartheta} = \frac{\vartheta+\chi(1-\vartheta)}{2-\vartheta-\chi(1-\vartheta)} = 1$. For NSF,

we will use the classical result (50), and also the simple result (49), which does not account for Knudsen layer corrections.

Since we are solving only the linearized equations, the DSMC simulations are performed for small deviations from equilibrium. Specifically, we prescribe the dimensionless temperatures of the liquid layers as $\theta_{0,1} = 1 \pm \Delta\theta$. The solutions depend strongly on the corresponding saturation pressures and we will show results for $\hat{p}_{sat}\left(\theta_L^{0,1}\right) = 1 \pm \Delta p$ with $\Delta\theta = 0.05$, $\Delta p = 0.05$ and $\Delta\theta = 0.01$, $\Delta p = 0.075$, respectively, where the second case produces the often discussed inverted temperature profile.[31] All results will be shown for a variety of Knudsen numbers in the range $\text{Kn} \in \{0.039, 1\}$.

With these data for temperature and pressure, the solutions of the linearized macroscopic equations yield profiles of temperature deviation and stress that are anti-symmetric relative to the midpoint $x = 0$. Although the deviations from equilibrium are small, the DSMC results show non-symmetric profiles due to small non-linearities. In order to have a proper comparison, we use not the original DSMC data but symmetrized temperature and stress profiles, which are obtained by appropriate averaging of the left and right parts of the profiles.

1. Standard temperature profile

When the dimensionless saturation pressures of the liquid layers are $\hat{p}_{sat}\left(\theta_L^{0,1}\right) = 1 \pm 0.05$, the temperature profile shows the expected behavior, with a jump at both boundaries

and, since the left boundary is hotter, a decreasing temperature in the bulk. Figures 2 and 3 show the temperature curve and the corresponding normal stress for Kn = 0.078 and Kn = 0.235, respectively, as functions of location x. Evidently, all macroscopic models have some difficulty in matching the full details of the temperature curve more so at larger Kn. Compared to DSMC, the NSF models give larger jumps at the boundaries (recall that the dimensionless liquid temperatures are $\theta_0 = 1.05$ and $\theta_1 = 0.95$, respectively) and a somewhat flatter temperature profile; they cannot describe normal stress ($\sigma = 0$). The R13 equations give jumps and temperature slopes close those of DSMC and give the normal stress in good approximation.

Maybe more important than the finer details of the profiles is the description of overall mass and heat transfer, that is, the dependence of the integration constants J_0 and q_0 on the Knudsen number. Figure 4 shows J_0, q_0, and the boundary stress $\sigma(x_1)$ for Knudsen numbers in $\{0, 1\}$, for DSMC (green dots), corrected NSF (blue dashed), uncorrected NSF (black dashed-dotted), and R13 (red continuous).

From the figure, we see that the corrected NSF equations (blue, dashed) give, for this problem, a good description of mass and heat transfer for all Knudsen numbers considered. As seen before, they do not give any non-equilibrium stress ($\sigma = 0$) and the temperature profiles do not match. That is, the accuracy in mass and heat flux is offset by the inaccurate temperature and stress profiles; it is not possible to adjust the
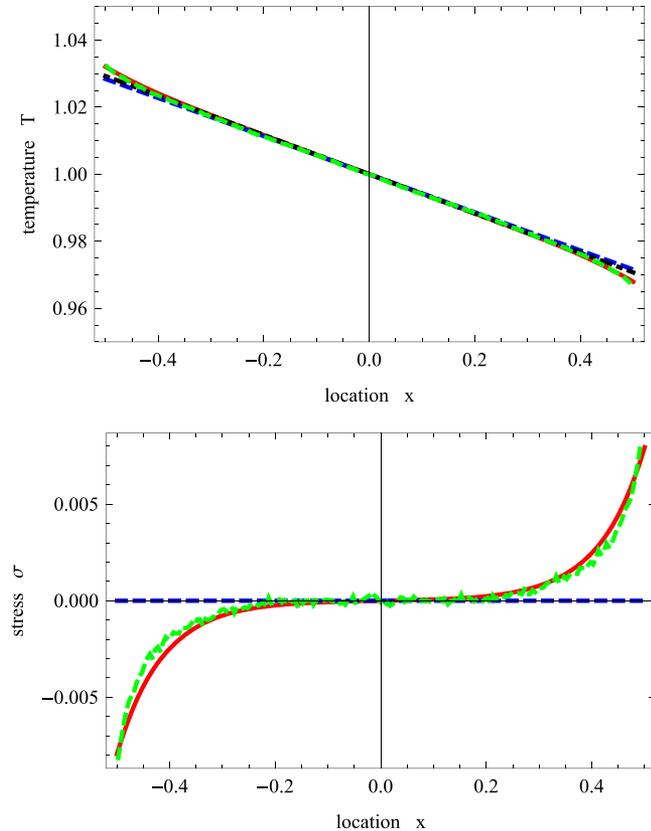

FIG. 2. Kn = 0.078: Temperature and stress profiles for $\Delta\theta = 0.05$ and $\Delta p = 0.05$, for DSMC simulation (symmetrized; green, dashed), corrected NSF (blue, dashed), uncorrected NSF (black, dotted-dashed), and R13 (red).
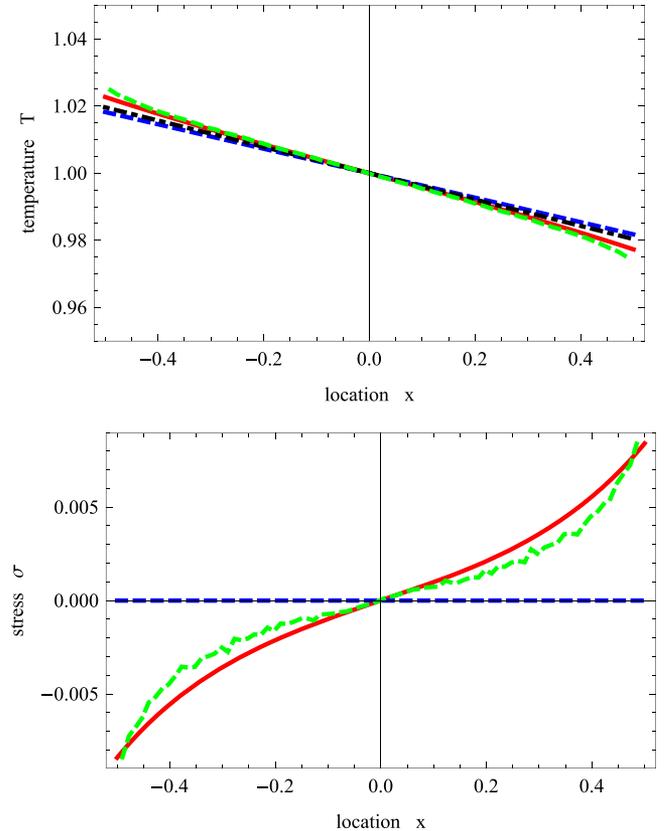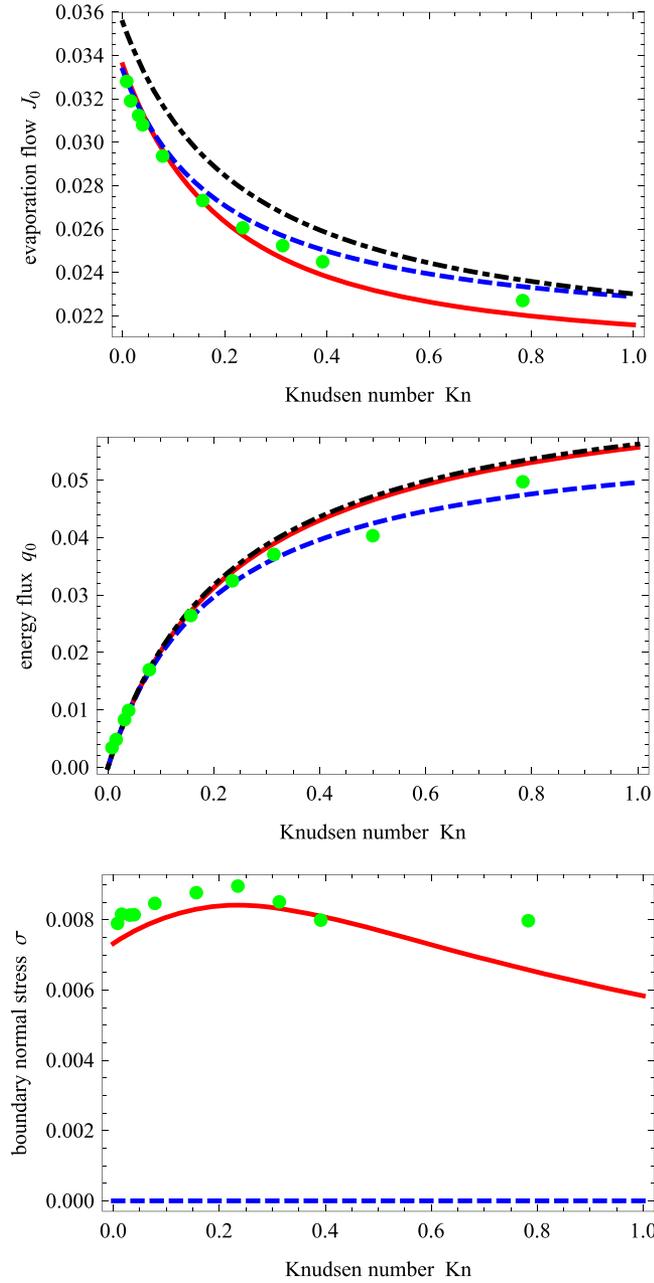
FIG. 3. Kn = 0.235: Temperature and stress profiles for $\Delta\theta = 0.05$ and $\Delta p = 0.05$, for DSMC simulation (symmetrized; green, dashed), corrected NSF (blue, dashed), uncorrected NSF (black, dotted-dashed), and R13 (red).

FIG. 4. Mass and heat transfer: Mass flow J_0 and heat flux q_0 as a function of the Knudsen number Kn, for $\Delta\theta = 0.05$ and $\Delta p = 0.05$: DSMC simulation (green, dots), corrected NSF (blue, dashed), uncorrected NSF (black, dotted-dashed), and R13 (red).

resistivities $\hat{r}_{\alpha\beta}$ to fit both fluxes and temperature profile. The uncorrected NSF equations (black, dashed-dotted), which do not correct Knudsen layer effects, do not provide a good match for fluxes or profiles.

The R13 equations (red, continuous) give a reasonable description of fluxes and stresses for relatively small Knudsen numbers (Kn $\leq$ 0.25), with relative errors for mass flux of less than 2%.

The visual fit for heat flux q_0 is good for all macroscopic systems, but it should be noted that for small Knudsen numbers, the energy flux q_0 is rather small, and there are fluctuations in the DSMC simulations, which leads to larger relative errors. According to (53), the total energy flux is

$Q_0 = \frac{5}{2} J_0 \theta_0 + q_0$, that is, energy transport—in particular at smaller Knudsen numbers—is dominated by convective transport. For the total energy flux Q_0, the corrected R13 equations differ from DSMC by not more than 1% for all Knudsen numbers considered, which is close to the accuracy of corrected NSF, where the relative error is below 0.9%.

2. Inverted temperature profile

Increase of the saturation pressure difference Δp for unchanged temperature difference $\Delta\theta$ implies an increase in the enthalpy of vaporization. For the transport between two liquid layers, this implies increased convective transport of energy or smaller conductive contribution to transport. For a certain range of values, and for the left liquid layer hotter than the right, it is possible that the temperature gradient in the bulk is inverted so that the vapor in front of the hotter liquid on the left is colder than the vapor in front of the colder liquid on the right.[31,34,35,52] It is worth mentioning that although a clear experimental evidence of temperature inversion during evaporation/condensation has not yet been given, inverted temperature profiles have been found in molecular dynamics simulations,[34] thus showing that their occurrence is not an artifact of kinetic boundary conditions. Temperature inversion occurs for DSMC simulations at $\Delta p = 0.075$ and $\Delta\theta = 0.01$, for which we show the same curves as before.
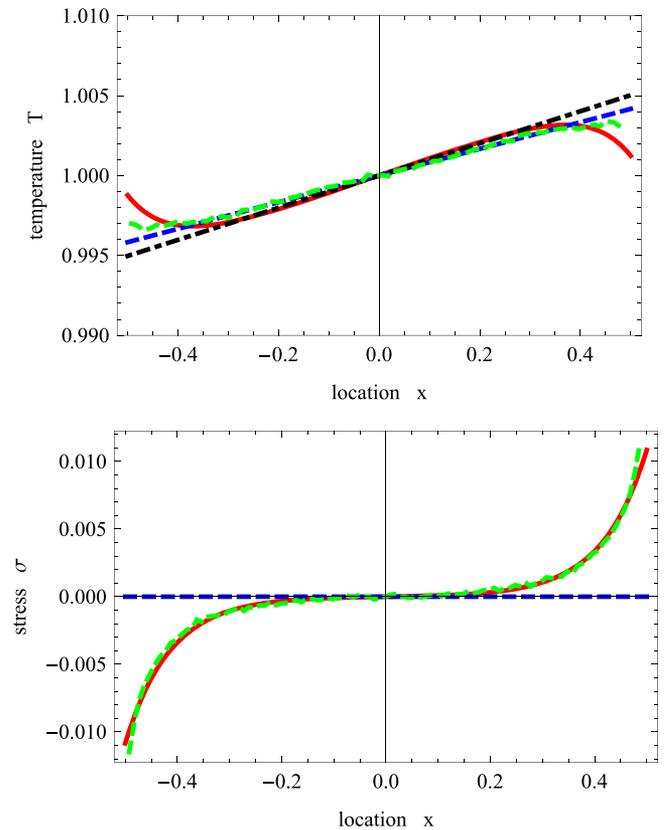

FIG. 5. Inverted temperature profile at Kn = 0.078: Temperature and stress profiles for $\Delta\theta = 0.01$ and $\Delta p = 0.075$, for DSMC simulation (symmetrized; green, dashed), corrected NSF (blue, dashed), uncorrected NSF (black, dotted-dashed), and R13 (red, continuous). Note that the liquid temperatures at the left and right are $\theta_0 = 1.01$ and $\theta_1 = 0.99$, respectively.

Figure 5 shows temperature and stress for Kn = 0.078. Note that the left and right temperatures are $\theta_0 = 1.01$ and $\theta_1 = 0.95$, respectively, which implies that the temperature jumps at the liquid-vapor interfaces are smaller than in the previous case ($\Delta p = 0.05$) and that the resolution of temperature is finer. Indeed, the R13 solutions show temperature Knudsen layer contributions due to the last term in Eq. (65)$_2$, which are present in Fig. 2 as well but, due to a different scale, hardly visible. As can be seen from Eq. (65), the Knudsen layer amplitude in temperature and the normal stress σ are both determined through the integration constant A. At a larger Knudsen number, e.g., at Kn = 0.235 as shown in Fig. 6, the amplitude A becomes so large that R13 fails to predict the inversion of the temperature profile, although the conductive heat flux, q_0, is inverted indeed, as can be seen in Fig. 7. NSF, on the other hand, describes the temperature profile fairly accurately but cannot describe the normal stress contribution.

The variation of mass flow J_0 and convective heat flux q_0 with the Knudsen number is shown in Fig. 7. Compared to Sec. IV C 1, we now have a larger mass flux and negative heat flux, that is, mass flux J_0 and total energy flux Q_0 point from the warm towards the cold liquid layer, but the conductive heat flux q_0 points in the opposite direction. As the figure shows, the boundary conditions for R13 (red) yield some deviation. Looking at the relative errors, we find that for Kn $\leq$ 0.4, corrected NSF predicts the mass flow with less than 0.5% deviation from the DSMC solutions and the heat flux q_0 with not

FIG. 7. Mass and heat transfer for inverted temperature profile: Mass flow J_0 and heat flux q_0 as a function of the Knudsen number Kn, for $\Delta\theta = 0.01$ and $\Delta p = 0.075$: DSMC simulation (green dots), corrected NSF (blue, dashed), uncorrected NSF (black, dotted-dashed), and R13 (red).

more than 10% deviation. The errors are larger for R13, with up to 2.1% for mass flux and up to 30% for heat flux; the total energy flux $Q_0 = \frac{5}{2}J_0 + q_0$, however, is predicted within 1.5%. Uncorrected NSF exhibits the largest overall errors, up to 7.5% for the mass flux and total energy flux.
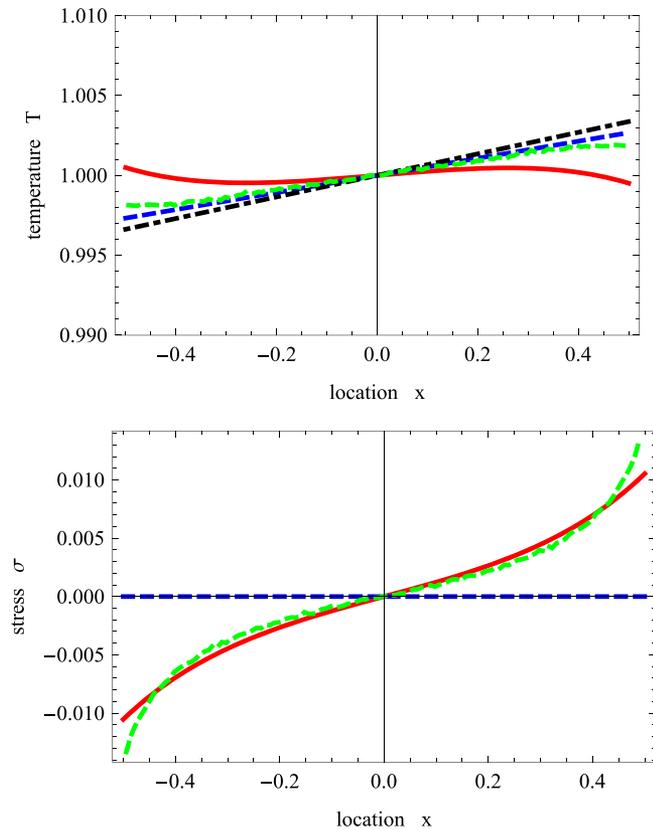

FIG. 6. Inverted temperature profile at Kn = 0.235: Temperature and stress profiles for $\Delta\theta = 0.01$ and $\Delta p = 0.075$, for DSMC simulation (symmetrized; green, dashed), corrected NSF (blue, dashed), uncorrected NSF (black, dotted-dashed), and R13 (red, continuous). Note that the liquid temperatures at the left and right are $\theta_0 = 1.01$ and $\theta_1 = 0.99$, respectively.
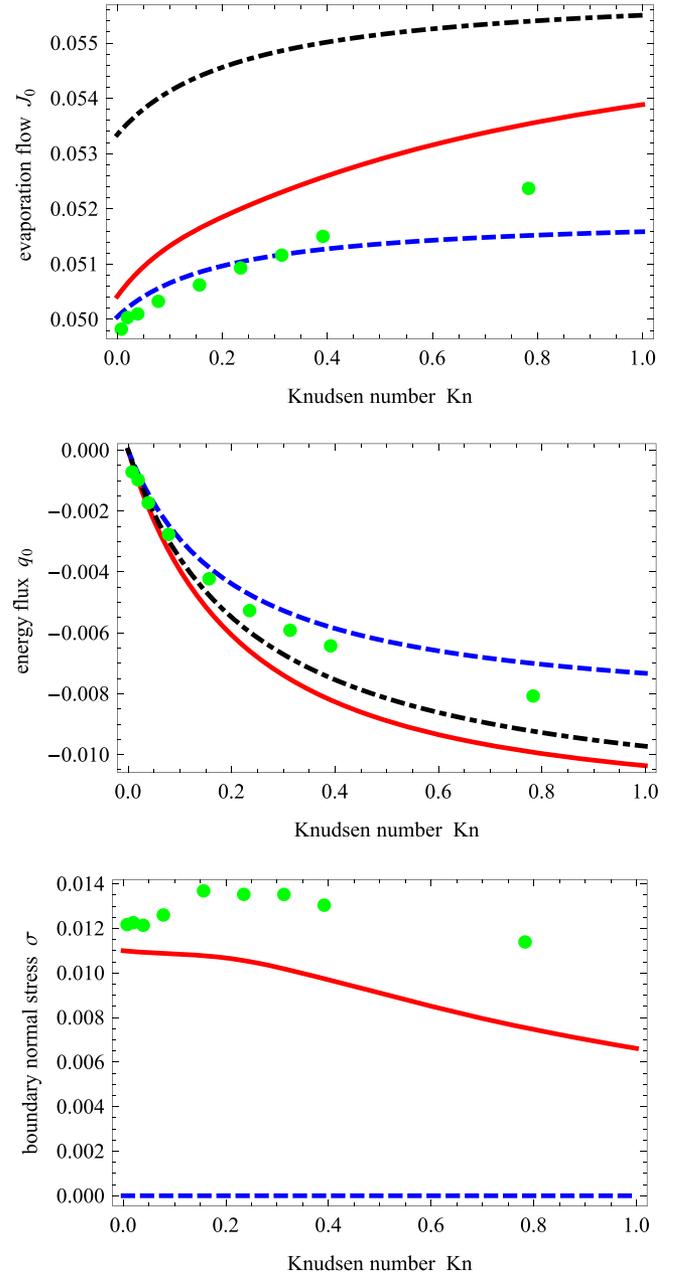
V. DISCUSSION AND CONCLUSIONS

In summary, our results indicate that the R13 equations with evaporation boundary conditions yield a qualitative description of the simple evaporation and condensation problems discussed here. In detail, however, they do not give perfect agreement.

From the shown data, one might conclude that the NSF equations with corrected boundary conditions give a more accurate description even for larger Knudsen numbers, but this is misleading. It must be kept in mind that flow problems in rarefied gases show a rich array of features, such as Knudsen layers, jump and slip, thermal stresses, thermal transpiration flow, heat flux without temperature gradient, etc., which are not accessible to the NSF theory, see Refs. [4] and [5] and references therein. The rich interplay between the different rarefaction effects comes into play in particular for multi-dimensional problems[8,37] but is mainly lost in the simple one-dimensional problems discussed above. Since R13 includes the rarefaction effects, and NSF does not, their predictions differ greatly in multidimensional problems. The good predictions of NSF for the problems discussed above are to some extent accidental, due to simple geometry. A case in point is the normal stress that R13 can reproduce in good accuracy but which is always zero for NSF.

By derivation, the NSF equations are valid only for rather small Knudsen numbers, and their good predictions for mass and energy fluxes for the problems considered here must be considered as circumstantial. Moreover, we note that the NSF interface conditions include fitted resistivities $r_{\alpha\beta}$, while the R13 boundary conditions are taken directly from the derivation of kinetic theory, without any *ad hoc* fitting coefficients. The NSF equations with uncorrected resistivities (49) give significantly larger errors than R13, which must be considered as a fitting-free improvement of the NSF equations.

Just as adjustment of interface resistivities gives a marked improvement for NSF, it is expected that the R13 predictions can be improved by adjusting the interface conditions. In Ref. [42], we introduced an Onsager matrix in the kinetic boundary conditions for R13 at non-absorbing walls, which lead to reasonable improvement, see also Ref. [53]. A similar procedure is possible here and will be explored in the future.

APPENDIX A: LIQUID PHASE AND CONSERVATION LAWS AT THE INTERFACE

In the bulk of the paper, we have considered only the gas phase (vapor), while the liquid phase only appeared in the interface conditions through its interface temperature θ_L and the corresponding saturation pressure $p_{\text{sat}}(\theta_L)$. For the problems that we have in mind for the future, such as evaporation of micro-droplets in micro-channels, the liquid phase can be assumed to be an incompressible liquid of constant mass density ρ_L, with constant specific heat c_L. The transport equations for the liquid phase then are simply the incompressible Navier-Stokes-Fourier equations, which read (sub-/super-script L denotes the liquid)

$$\frac{\partial v_k^L}{\partial x_k} = 0,$$

$$\rho_L \frac{Dv_i^L}{Dt} + \frac{\partial p_L}{\partial x_i} + \frac{\partial \sigma_{ik}^L}{\partial x_k} = 0, \tag{A1}$$

$$\rho_L c_L \frac{D\theta_L}{Dt} + \frac{\partial q_k^L}{\partial x_k} + \sigma_{kl}^L \frac{\partial v_k^L}{\partial x_l} = 0,$$

with the respective laws for stress and heat flux,

$$\sigma_{ij}^L = -2\mu_L \frac{\partial v_{\langle i}^L}{\partial x_{j\rangle}}, \quad q_i^L = -\kappa_L \frac{\partial \theta_L}{\partial x_i}. \tag{A2}$$

Here, μ_L and κ_L are the liquid's viscosity and heat conductivity, respectively.

The conservation laws for mass, momentum, and energy for the gas (2) and the vapor (A1) hold in the respective bulk phases. For a complete description, we also require the conservation laws at the interface. The easiest model of the interface is a massless interface without surface tension and surface energy. As before, we consider an interface that moves with the velocity v_i^I and is characterized by the normal vector n_i that points from the liquid towards the gas. For such an interface, the conservation laws of mass, momentum, and energy declare the continuity of the normal fluxes for an observer resting on the interface. With the liquid properties on the left, and the gas properties on the right, these can be written as[54]

$$\left[\rho_L\left(v_j^L - v_j^I\right)\right] n_j = \left[\rho\left(v_j - v_j^I\right)\right] n_j, \tag{A3}$$

$$\left[\rho_L v_i^L \left(v_j^L - v_j^I\right) + p_L \delta_{ij} + \sigma_{ij}^L\right] n_j$$
$$= \left[\rho v_i \left(v_j - v_j^I\right) + p\delta_{ij} + \sigma_{ij}\right] n_j, \tag{A4}$$

$$\left[\rho_L\left(h_L + \frac{1}{2}v_L^2\right)\left(v_j^L - v_j^I\right) + p_L v_j^L + \sigma_{ij}^L v_i^L + q_j^L\right] n_j$$

$$= \left[\rho\left(h + \frac{1}{2}v^2\right)\left(v_j - v_j^I\right) + p v_j + \sigma_{ij} v_i + q_j\right] n_j, \tag{A5}$$

where $h = u + \frac{p}{\rho}$ denotes the enthalpy. Surface tension effects must be added for curved surfaces, such as droplets or bubbles.[54]

At sufficiently low pressures, liquid enthalpy can be approximated as

$$h_L = c_L \theta - h_0 \tag{A6}$$

with an enthalpy constant h_0 that must be carefully chosen in order to incorporate the latent heat into the model. Indeed, in kinetic theory, the enthalpy of the (monatomic) vapor is

$$h = u + \frac{p}{\rho} = \frac{5}{2}\theta = c_p \theta \tag{A7}$$

so that the heat of vaporization is

$$h_{LV}(\theta) = h - h_L = h_0 - \left(c_L - c_p\right)\theta. \tag{A8}$$

Due to the simplicity of the model, only one value of the heat of vaporization is required to fit the constant h_0. With a reference value $h_{LV}^0 = h_{LV}(\theta_0)$, we have $h_0 = h_{LV}^0 + \left(c_L - c_p\right)\theta_0$, hence the enthalpy of the liquid and the enthalpy of vaporization are

$$h_L = c_L\left(\theta - \theta_0\right) + c_p\theta_0 - h_{LV}^0, \tag{A9}$$

$$h_{LV}(\theta) = h_{LV}^0 - \left(c_L - c_p\right)\left(\theta - \theta_0\right). \tag{A10}$$

In Ref. 49, it is shown that this simple model—vapor as ideal gas and liquid as incompressible ideal liquid, both with constant specific heats—leads to an explicit expression for saturation pressure that in the present notation reads as

$$p_{\text{sat}}(\theta) = p_{\text{sat}}(\theta_0) \exp\left[\left(c_L - c_p\right)\left(1 - \frac{\theta_0}{\theta} - \ln\left(\frac{\theta}{\theta_0}\right)\right) + h_{LV}^0\left(\frac{1}{\theta_0} - \frac{1}{\theta}\right)\right]. \quad \text{(A11)}$$

Note that we have absorbed the gas constant R into temperature as $\theta = RT$, hence the specific heats c_L and $c_p = \frac{5}{2}$ are dimensionless; $p_{\text{sat}}(\theta_0)$ is the saturation pressure at reference temperature θ_0.

APPENDIX B: DETAILS OF DSMC CALCULATIONS

Reference flow field profiles, both for evaporation into a half space and for the evaporation/condensation between two parallel plates, have been obtained by DSMC simulations of a monatomic vapor. The code is based on a quite standard implementation of Koura's *null-collision* estimator of collision rate.[55] The presented profiles are based on hard spheres simulations. A smaller number of computationally more expensive Maxwell molecule simulations showed very little variation with respect to hard spheres profiles, once the two model cross sections have been tuned on the same viscosity at the reference temperature, for the problem at hand. It should be observed that in both problems, temperature variations are extremely small; hence, the different viscosity temperature exponents of the two collision models are not seen in the simulations.

Boundary conditions at evaporating/condensing liquid surfaces have been assigned by assuming the unit evaporation/condensation coefficient and Maxwellian distribution function of evaporating molecules, characterized by the liquid surface temperature θ_L and the saturated vapor density $n_{sat}(\theta_L)$. In the case of the evaporation into a half space, the boundary condition at infinity requires some care since the asymptotic Maxwellian state is not known but it is a result of the simulation. Taking into account that the density and temperature at infinity are determined by the downstream Mach number (or flow speed), the correct equilibrium state can be determined by the boundary condition formulated in Ref. 56.

In order to match the linearized R13 regime, DSMC has been used to study small departures from equilibrium. The one-dimensional computational domain has been divided into a number of cells of the same size, not larger that $\lambda_0/10$, λ_0 being the equilibrium mean free path. Not less than 3000 particles per cell have been used, in order to capture small deviations from equilibrium. Typically, each simulation has been started from a given spatially uniform equilibrium state. Sampling of macroscopic quantities has been started after the onset of steady flow conditions, the sampling time duration being determined by the estimated relative statistical error. The latter does not exceed 0.01. The highest computing time has been equal to about 26 h on a single processor in a case in which the Knudsen number has been set equal to 1/100, the number of particles is equal to 3×10^6, and the number of time steps is equal to 3.2×10^5. Smaller or much smaller computational effort is required for larger Knudsen numbers because of the smaller particle number and shorter transient duration.

[1] H. Struchtrup and M. Torrilhon, "Regularization of Grad's 13 moment equations: Derivation and linear analysis," Phys. Fluids **15**(9), 2668–2680 (2003).

[2] M. Torrilhon and H. Struchtrup, "Regularized 13-moment equations: Shock structure calculations and comparison to Burnett models," J. Fluid Mech. **513**, 171–198 (2004).

[3] H. Struchtrup, *Macroscopic Transport Equations for Rarefied Gas Flows— Approximation Methods in Kinetic Theory*, Interaction of Mechanics and Mathematics Series (Springer, Heidelberg, 2005).

[4] H. Struchtrup and P. Taheri, "Macroscopic transport models for rarefied gas flows: A brief review," IMA J. Appl. Math. **76**(5), 672–697 (2011).

[5] M. Torrilhon, "Modeling nonequilibrium gas flow based on moment equations," Annu. Rev. Fluid Mech. **48**, 429–458 (2016).

[6] S. Chapman and T. G. Cowling, *The Mathematical Theory of Non-Uniform Gases* (Cambridge University Press, 1970).

[7] C. Cercignani, *Theory and Application of the Boltzmann Equation* (Scottish Academic Press, Edinburgh, 1975).

[8] A. Mohammadzadeh, A. S. Rana, and H. Struchtrup, "Thermal stress vs. thermal transpiration: A competition in thermally driven cavity flows," Phys. Fluids **27**, 112001 (2015).

[9] G. Bird, *Molecular Gas Dynamics and the Direct Simulation of Gas Flows* (Clarendon Press, Oxford, 1994).

[10] L. Mieussens, "A survey of deterministic solvers for rarefied flows," AIP Conf. Proc. **1628**, 943–951 (2014).

[11] H. Struchtrup, "Derivation of 13 moment equations for rarefied gas flow to second order accuracy for arbitrary interaction potentials," Multiscale Model. Simul. **3**(1), 221–243 (2005).

[12] H. Struchtrup, "Stable transport equations for rarefied gases at high orders in the Knudsen number," Phys. Fluids **16**(11), 3921–3934 (2004).

[13] H. Grad, "On the kinetic theory of rarefied gases," Commun. Pure Appl. Math. **2**, 331–407 (1949).

[14] H. Grad, "Principles of the kinetic theory of gases," in *Handbuch der Physik XII: Thermodynamik der Gase*, edited by S. Flügge (Springer, Berlin, 1958).

[15] D. Burnett, "The distribution of molecular velocities and the mean motion in a non-uniform gas," Proc. London Math. Soc. **s2-40**, 382–435 (1936).

[16] M. Sh. Shavaliyev, "Super-Burnett corrections to the stress tensor and the heat flux in a gas of Maxwellian molecules," J. Appl. Math. Mech. **57**(3), 573–576 (1993).

[17] A. V. Bobylev, "The Chapman-Enskog and Grad methods for solving the Boltzmann equation," Sov. Phys. Dokl. **27**, 29–31 (1982).

[18] P. Rosenau, "Extending hydrodynamics via the regularization of the Chapman-Enskog solution," Phys. Rev. A **40**, 7193–7196 (1989).

[19] H. Struchtrup, "Some remarks on the equations of Burnett and Grad," *Transport in Transition Regimes*, IMA (Springer, New York, 2003), Vol. 135.

[20] W. Weiss, "Continuous shock structure in extended thermodynamics," Phys. Rev. E **52**, R5760–R5763 (1995).

[21] X. J. Gu and D. R. Emerson, "A high-order moment approach for capturing non-equilibrium phenomena in the transition regime," J. Fluid Mech. **636**, 177–216 (2009).

[22] M. Torrillhon, "Convergence study of moment approximations for boundary value problems of the Boltzmann-BGK equation," Commun. Comput. Phys. **18**(3), 529–557 (2015).

[23] H. Struchtrup and M. Torrilhon, "Regularized 13 moment equations for hard sphere molecules: Linear bulk equations," Phys. Fluids **25**, 052001 (2013).

[24] B. Rahimi and H. Struchtrup, "Capturing non-equilibrium phenomena in rarefied polyatomic gases: A high-order macroscopic model," Phys. Fluids **26**, 052001 (2014).

[25] V. K. Gupta, H. Struchtrup, and M. Torrilhon, "Regularized moment equations for binary gas mixtures: Derivation and linear analysis," Phys. Fluids **28**, 042003 (2016).

[26] M. Torrilhon and H. Struchtrup, "Boundary conditions for regularized 13-moment-equations for micro-channel-flows," J. Comput. Phys. **227**, 1982–2011 (2008).

[27] J. C. Maxwell, "On stresses in rarified gases arising from inequalities of temperature," Philos. Trans. R. Soc. **170**, 231–256 (1879).

[28] J. P. Caputa and H. Struchtrup, "Interface model for non-equilibrium evaporation," Physica A **390**, 31–42 (2011).

[29] T. Ytrehus, *Kinetic Theory Description and Experimental Results for Vapor Motion in Arbitrary Strong Evaporation*, Technical Note 112 (von Karman Institute for Fluid Dynamics, 1975).

[30] Y. Sone, "Kinetic theoretical studies of the half-space problem of evaporation and condensation," Transp. Theory Stat. Phys. **29**, 227–260 (2000).

[31] Y. P. Pao, "Application of kinetic theory to the problem of evaporation and condensation," Phys. Fluids **14**, 306–312 (1971).

[32] Y. P. Pao, "Temperature and density jumps in the kinetic theory of gases and vapors," Phys. Fluids **14**, 1340–1346 (1971).

[33] J. W. Cipolla, H. Lang, and S. K. Loyalka, "Kinetic theory of condensation and evaporation. II," J. Chem. Phys. **61**, 69–78 (1974).

[34] A. Frezzotti, P. Grosfils, and S. Toxvaerd, "Evidence of an inverted temperature gradient during evaporation/condensation of a Lennard-Jones fluid," Phys. Fluids **15**, 2837–2842 (2003).

[35] H. Struchtrup, S. Kjelstrup, and D. Bedeaux, "Temperature-difference-driven mass transfer through the vapor from a cold to a warm liquid," Phys. Rev. E **85**, 061201 (2012).

[36] H. Struchtrup and A. Frezzotti, "Evaporation/condensation boundary conditions for the regularized 13 moment equations," AIP Conf. Proc. **1786**, 140002 (2016).

[37] A. S. Rana, M. Torrilhon, and H. Struchtrup, "A robust numerical method for the R13 equations of rarefied gas dynamics: Application to lid driven cavity," J. Comput. Phys. **236**, 169–186 (2013).

[38] M. Yu. Timokhin, H. Struchtrup, A. A. Kokhanchik, and Ye. A. Bondar, "Different variants of R13 moment equations applied to the shock-wave structure," Phys. Fluids **29**, 037105 (2017).

[39] P. L. Bhatnagar, E. P. Gross, and M. Krook, "A model for collision processes in gases. I. Small amplitude processes in charged and neutral one-component systems," Phys. Rev. **94**, 511–525 (1954).

[40] I. Kuscer and M. Robnik, "Semi-microscopic description of evaporation and condensation," J. Phys. A: Math. Gen. **13**, 621 (1980).

[41] K. W. Kolasinski, *Surface Science* (Wiley, Hoboken, 2008).

[42] A. S. Rana and H. Struchtrup, "Thermodynamically admissible boundary conditions for the regularized 13 moment equations," Phys. Fluids **28**, 027105 (2016).

[43] H. Struchtrup, "Linear kinetic heat transfer: Moment equations, boundary conditions, and Knudsen layers," Physica A **387**, 1750–1766 (2008).

[44] S. R. de Groot and P. Mazur, *Non-Equilibrium Thermodynamics* (Dover, 1984).

[45] S. Kjelstrup, D. Bedeaux, E. Johannessen, and J. Gross, *Non-Equilibrium Thermodynamics for Engineers* (World Scientific, 2010).

[46] H. Hertz, "Über die Verdunstung der Flüssigkeiten, insbesondere des Quecksilbers, im luftleeren Raume," Ann. Phys. **253**, 177–193 (1882).

[47] M. Knudsen, "Die maximale Verdampfungsgeschwindigkeit des Quecksilbers," Ann. Phys. **352**, 697–708 (1915).

[48] R. W. Schrage, *A Theoretical Study of Interphase Mass Transfer* (Columbia University Press, New York, 1953).

[49] M. Bond and H. Struchtrup, "Mean evaporation and condensation coefficients based on energy dependent condensation probability," Phys. Rev. E **70**, 061605 (2004).

[50] S. Kjelstrup and D. Bedeaux, *Non-Equilibrium Thermodynamics of Heterogeneous Systems* (World Scientific, 2008).

[51] J. B. Young, "Calculation of Knudsen layers and jump conditions using the linearised G13 and R13 moment methods," Int. J. Heat Mass Transfer **54**, 2902–2912 (2012).

[52] H. Struchtrup, S. Kjelstrup, and D. Bedeaux, "Analysis of temperature difference driven heat and mass transfer in the Phillips-Onsager cell," Int. J. Heat Mass Transfer **58**, 521–531 (2013).

[53] M. Torrilhon and N. Sarna, "Hierarchical Boltzmann simulations and model error estimation," J. Comput. Phys. **342**, 66–84 (2017).

[54] I. Müller, *Thermodynamics* (Pitman, Boston, 1985).

[55] K. Koura, "Null-collision technique in the direct simulation Monte Carlo method," Phys. Fluids **29**, 3509–3511 (1986).

[56] A. Frezzotti, in *Kinetic Theory Description of the Evaporation of Multi-Component Substances, Proceedings of the 20th International Symposium on Rarefied Gas Dynamics* (Peking University Press, 1997), pp. 837–846.